The *Pseudomonas aeruginosa* LasR quorum-sensing receptor balances ligand selectivity and sensitivity

Amelia R. McCready[1], Jon E. Paczkowski[1], Brad R. Henke[2], and Bonnie L. Bassler[1,3,4]

Running Title: LasR balances sensitivity and selectivity

Keywords: crystal structure / LasR / *Pseudomonas aeruginosa* / quorum sensing / receptor specificity

From: The Department of Molecular Biology, Princeton University, Princeton, NJ 08544[1], Opti-Mol Consulting, LLC, Cary, NC 27513[2], Howard Hughes Medical Institute, Chevy Chase, MD 20815[3]

[4]To whom correspondence should be addressed: Prof. Bonnie L. Bassler, Department of Molecular Biology, Princeton University, 329 Lewis Thomas Laboratory, Princeton, NJ 08544.

Email:bbassler@princeton.edu

Abstract

Quorum sensing is a cell-cell communication process that bacteria use to orchestrate group behaviors. Quorum sensing is mediated by extracellular signal molecules called autoinducers. Autoinducers are often structurally similar, raising questions concerning how bacteria distinguish among them. Here, we use the *Pseudomonas aeruginosa* LasR quorum-sensing receptor to explore receptor sensitivity and selectivity. Alteration of LasR amino acid S129 increases ligand selectivity and decreases ligand sensitivity. Conversely, the L130F mutation enhances LasR sensitivity while reducing selectivity. We solve crystal structures of LasR ligand binding domains complexed with non-cognate autoinducers. Comparison to existing structures reveals that ligand selectivity/sensitivity is mediated by a flexible loop adjacent to the ligand binding site. We show that *P. aeruginosa* harboring LasR variants with modified selectivity or sensitivity exhibit altered quorum-sensing responses. We suggest that an evolutionary trade-off between ligand selectivity and sensitivity enables LasR to optimally regulate quorum-sensing traits.

Introduction

Quorum sensing is a cell-cell communication process that enables bacteria to collectively control behavior (reviewed in Papenfort & Bassler, 2016). Quorum sensing relies on the production, release, and detection of extracellular signal molecules called autoinducers (Albus, Pesci, RunyenJanecky, West, & Iglewski, 1997; Engebrecht, Nealson, & Silverman, 1983; Latifi et al., 1995). At low cell density, autoinducer

23 concentration is low, and bacteria act as individuals. As cell density increases,
24 autoinducer concentration also rises. Under this condition, autoinducers bind to cognate
25 receptors, initiating the population-wide regulation of genes underlying collective
26 behaviors.

27 Many species of Gram-negative bacteria use acylated homoserine lactones
28 [HSLs] as autoinducers (Brint & Ohman, 1995; Cao & Meighen, 1989; Eberhard et al.,
29 1981; Hanzelka et al., 1999; Pearson et al., 1994). HSL autoinducers possess identical
30 lactone head groups, but they vary in acyl tail length and decoration. The tail modifications
31 promote specificity between particular HSL autoinducers and partner receptors (Churchill
32 & Chen, 2011). There are two kinds of HSL autoinducer receptors. First, there are LuxR-
33 type receptors, which are cytoplasmic HSL-binding transcription factors that possess
34 variable ligand binding domains [LBD] and well-conserved helix-turn-helix DNA binding
35 domains [DBD] (Nasser & Reverchon, 2007; Vannini et al., 2002). There are also LuxN-
36 type receptors, which are membrane-spanning two-component signaling proteins that
37 bind HSL ligands in their periplasmic regions and transduce information regarding ligand
38 occupancy internally by phosphorylation/dephosphorylation cascades (Bassler, Wright,
39 Showalter, & Silverman, 1993; Freeman, Lilley, & Bassler, 2000; reviewed in Papenfort
40 & Bassler, 2016).

41 Ligand sensitivity and selectivity has been examined in the founding member of
42 the LuxN receptor family from *Vibrio harveyi* (Ke, Miller, & Bassler, 2015). LuxN is
43 exquisitely selective for its cognate autoinducer $3OHC_4HSL$. Specific amino acids were
44 identified in the predicted LuxN transmembrane spanning region that confer selectivity for

45 tail length and for tail decoration. Longer HSLs competitively inhibit LuxN, suggesting that,
46 in mixed-species consortia, *V. harveyi* monitors the vicinity for competing species, and in
47 response to their presence, exploits LuxN antagonism to delay the launch of its quorum-
48 sensing behaviors, thus avoiding loss of expensive public goods to non-kin.

49 Some analyses of ligand preference in LuxR-type receptors have been performed.
50 TraR from *Agrobacterium tumefaciens* excludes non-native HSLs (Hawver, Jung, & Ng,
51 2016; Vannini et al., 2002; You et al., 2006; Zhu & Winans, 2001), LasR from
52 *Pseudomonas aeruginosa* detects several long chain HSLs (Gerdt et al., 2017), and SdiA
53 from *Escherichia coli* is highly promiscuous and avidly responds to HSLs with variable
54 chain lengths (Michael, Smith, Swift, Heffron, & Ahmer, 2001; Nguyen et al., 2015;
55 Sitnikov, Schineller, & Baldwin, 1996). Comparison of structures of the LasR and TraR
56 LBDs suggests that increased hydrogen bonding to the ligand in TraR, compared to LasR,
57 accounts for the selectivity difference (Gerdt et al., 2017). Here, we systematically explore
58 the LasR response to $3OC_{12}HSL$ and non-native HSLs with respect to selectivity and
59 sensitivity. We use mutagenesis to establish the amino acid determinants that enable
60 LasR to discriminate between HSLs. We identify LasR S129 as the amino acid residue
61 that, when altered, improves LasR selectivity for HSLs by restricting the set of HSLs
62 capable of activation. Mutations at LasR S129, however, reduce overall affinity for HSL
63 ligands. In contrast, we find that LasR L130F exhibits diminished ligand selectivity,
64 responding to a broader set of HSLs than wildtype LasR, with enhanced sensitivity.
65 Altering LasR sensitivity or selectivity affects the timing and strength of quorum-sensing
66 control of *P. aeruginosa* behaviors. Finally, we solve crystal structures of the LasR LBD

67 L130F bound to non-native autoinducers to establish the structural basis underlying
68 ligand selectivity and sensitivity. We find that a flexible loop located near the ligand
69 binding pocket promotes ligand promiscuity in the wildtype protein. This loop exists in
70 SdiA, which is promiscuous, but not in TraR which is highly specific for its cognate ligand.
71 We propose that there is a trade-off between ligand selectivity and sensitivity in LasR and
72 evolution has established a balance between ligand discrimination and ligand sensitivity.
73 Because LasR requires higher concentrations of non-cognate autoinducers than its
74 cognate autoinducer for activation, this tradeoff could allow LasR to robustly respond to
75 its own signal molecule, even in the presence of other bacteria that are producing HSL
76 autoinducers. Nonetheless, *P. aeruginosa* would be capable of reacting to the presence
77 of these other bacteria when it is outnumbered.
78

79 **Results**

80 <u>LasR responds to multiple HSL autoinducers</u>

81 To investigate the preference LasR displays for different HSLs, we employed a plasmid
82 reporter system in which transcription from a LasR-controlled promoter fused to luciferase
83 (p*lasB-lux*) was assessed in *E. coli*. Arabinose-inducible *lasR* was cloned on a second
84 plasmid (Paczkowski et al., 2017; Pearson, Pesci, & Iglewski, 1997). A set of HSLs
85 differing in both carbon chain length and in functionality at the C-3 carbon were
86 synthesized using a modification of a previously reported method (Chhabra et al., 2003)
87 (see Appendix). Figure 1A shows reporter output following addition of 100 nM of the
88 cognate autoinducer, $3OC_{12}HSL$, and four other HSLs ($3OC_{14}HSL$, $3OC_{10}HSL$,

89 3OC$_8$HSL, and 3OC$_6$HSL). All five HSLs activated LasR, but to differing levels.
90 3OC$_{12}$HSL, 3OC$_{14}$HSL, and 3OC$_{10}$HSL elicited maximal LasR activity, and 3OC$_8$HSL and
91 3OC$_6$HSL stimulated 7-fold and 18-fold less activity, respectively. We examined 8 other
92 HSLs harboring different functionalities on the C-3 carbon in combination with the various
93 tail lengths. Using dose-response analyses, we obtained EC$_{50}$ values for the compounds
94 (Table 1 and Table S1). 3OC$_{12}$HSL was the most potent ligand, with an EC$_{50}$ of
95 approximately 2.8 nM. 3OC$_{14}$HSL was half as potent with an EC$_{50}$ of 5.6 nM. From there,
96 the EC$_{50}$ values followed the order 3OC$_{10}$HSL < 3OC$_8$HSL < 3OC$_6$HSL. Table EV1 shows
97 the remainder of the data and that the ketone versions of the molecules are the most
98 potent for every chain length. For this reason, we used the five HSLs shown in Table 1
99 for much of the remainder of this work. We measured *in vivo* LasR activity in response to
100 the test HSLs using an elastase assay (Gambello & Iglewski, 1991). Elastase is encoded
101 by *lasB*, and as a reminder, we employed the *lasB* promoter in the *E. coli* reporter assay.
102 For the elastase analyses, we used a Δ*lasI P. aeruginosa* strain that makes no
103 endogenous 3OC$_{12}$HSL. When supplied at 100 nM, all of the test compounds elicited
104 some elastase activity, but 3OC$_{12}$HSL stimulated the highest elastase production (Figure
105 1B). We do note that in *P. aeruginosa*, 3OC$_{14}$HSL and 3OC$_8$HSL stimulated lower activity
106 than expected based on their EC$_{50}$ values in *E. coli.* Indeed, as shown below, these two
107 molecules had reduced activity in all assays in all *P. aeruginosa* strains used here. While
108 we do not know the underlying molecular mechanism, we suspect that perhaps there is
109 reduced permeability into *P. aeruginosa* and/or there is a factor in *P. aeruginosa* that does
110 not exist in *E. coli* that binds and titrates out these two molecules. Nonetheless, our results

111 indicate that, at least with respect to the HSLs we tested, *in vivo,* LasR is most active in
112 response to its cognate autoinducer $3OC_{12}HSL$, but non-cognate HSLs can induce
113 production of the quorum-sensing product elastase, and presumably other quorum-
114 sensing regulated outputs.

115 LasR and most other LuxR-type receptors fold around their cognate HSL ligands.
116 Thus, they are only soluble, capable of dimerizing, and binding DNA when ligand is
117 present (Bottomley, Muraglia, Bazzo, & Carfi, 2007; Zhu & Winans, 2001). The results in
118 Figure 1A and 1B suggest that LasR can fold around HSLs in addition to $3OC_{12}HSL$. To
119 verify this notion, we tested whether LasR could be solubilized by non-native HSLs. To
120 do this, we grew *E. coli* producing the LasR LBD in the presence of the 13 HSL
121 compounds (Figure 1C shows the five test compounds and Figure EV1A shows the eight
122 other compounds in the collection). Consistent with previous results, in the absence of
123 any ligand (DMSO control), the LasR LBD is present in the whole cell lysate, but not in
124 the soluble fraction indicating that the protein is insoluble (O'Loughlin et al., 2013;
125 Schuster, Urbanowski, & Greenberg, 2004). All five of the HSL test compounds except
126 for $3OC_6HSL$ solubilized the LasR LBD (Figure 1C). Nonetheless, we could only purify to
127 homogeneity the LasR LBD bound to the ligands containing the longer acyl tails:
128 $3OC_{12}HSL$, $3OC_{14}HSL$, and $3OC_{10}HSL$. Together, the results in Figure 1 suggest that
129 although $3OC_8HSL$ and $3OC_6HSL$ can bind to and activate LasR, their interactions must
130 be more transient than ligands with longer acyl tails. To garner evidence for this idea, we
131 performed thermal shift analyses on LasR LBD-ligand complexes without and with the
132 addition of either the same or a different HSL. The LasR LBD bound to $3OC_{10}HSL$,

133 3OC$_{12}$HSL, and 3OC$_{14}$HSL had melting temperatures of 42.3 ^{o}C, 49.1 ^{o}C, and 50.5 ^{o}C,
134 respectively (Figure 2, black lines) showing that LasR stability increases with increasing
135 ligand tail length. Notably, the LasR LBD is more stable when bound to the non-cognate
136 ligand 3OC$_{14}$HSL than when bound to the cognate ligand 3OC$_{12}$HSL. The discrepancy
137 between the enhanced stability of purified LasR LBD:3OC$_{14}$HSL relative to 3OC$_{12}$HSL in
138 the thermal shift assay and the higher EC$_{50}$ for 3OC$_{14}$HSL compared to 3OC$_{12}$HSL could
139 result from increased hydrophobic interactions in the stably purified complex that do not
140 drive activation and affinity of LasR for a particular ligand.

141 Exogenously supplied autoinducers can shift the melting temperature of an
142 existing receptor-ligand complex if the added ligand has the ability to stabilize the
143 unfolding protein as it releases the pre-bound ligand. Importantly, exogenously supplied
144 HSLs can only stabilize the LasR LBD if they have affinities that are equal to or higher
145 than the originally bound ligand (Paczkowski et al., 2017). In the case of the LasR
146 LBD:3OC$_{10}$HSL complex, when added exogenously, the ligands 3OC$_{10}$HSL, 3OC$_{12}$HSL,
147 and 3OC$_{14}$HSL stabilize the LasR LBD, increasing the melting temperature 3.4 ^{o}C, 6.4
148 ^{o}C, and 5.5 ^{o}C, respectively (Figure 2). By contrast, the LasR LBD:3OC$_{12}$HSL and the
149 LasR LBD:3OC$_{14}$HSL complexes could only be further stabilized by exogenously supplied
150 3OC$_{12}$HSL and 3OC$_{14}$HSL, but not by 3OC$_{10}$HSL, indicating that the association rate of
151 3OC$_{10}$HSL for the LasR LBD is slower than that of 3OC$_{12}$HSL and 3OC$_{14}$HSL (Figure 2).
152 While the short acyl chain HSLs were capable of activation of LasR with high micromolar
153 EC$_{50}$ values in the p*lasB-lux* reporter assay, 3OC$_{6}$HSL and 3OC$_{8}$HSL did not stabilize the
154 LasR LBD protein sufficiently in *E. coli*, presumably due to their low affinities (Figure 1C

155 and Table 1). Thus, they could not be tested in the traditional thermal shift assay. They
156 also did not enhance the stabilization of the LasR LBD pre-bound with other ligands,
157 analogous to the inability of $3OC_{10}HSL$ to stabilize the LasR LBD:$3OC_{12}HSL$ complex as
158 it melted (Figure 2). Together, our results indicate that in an environment containing a
159 mixture of HSL autoinducers, LasR will preferentially detect long chain HSLs, with
160 superior preference for its own autoinducer $3OC_{12}HSL$, followed closely by $3OC_{14}HSL$.
161
162 <u>LasR S129 drives ligand selectivity and sensitivity.</u>
163 To understand how LasR selects HSL ligands with which to interact, we performed
164 site directed mutagenesis guided by the existing crystal structure of the LasR LBD bound
165 to $3OC_{12}HSL$ (Bottomley et al., 2007). We first focused on residue S129. Previous work
166 has demonstrated that alteration of serine to alanine at this site enables some synthetic
167 LasR activators to transform into inhibitors and vice-versa (Gerdt, McInnis, Schell, &
168 Blackwell, 2015; Gerdt, McInnis, Schell, Rossi, & Blackwell, 2014). Moreover, the LasR
169 LBD structure suggests that S129 is part of the network that interacts with the ligand acyl
170 tail (Bottomley et al., 2007). For these reasons, we predicted that S129 could contribute
171 to LasR selectivity. We constructed LasR S129C, S129W, S129F, S129T, and S129M
172 and examined their activities in the *E. coli* p*lasB-lux* reporter system. Table 1 shows the
173 EC_{50} values for all of the mutants and the five test compounds. The EC_{50} values follow
174 the order: wildtype < LasR S129C < LasR S129W < LasR S129F < LasR S129T < LasR
175 S129M. We note there are two exceptions to this trend among the low affinity interactions
176 (Table 1). However, in those cases, the EC_{50} values are high and we suspect that the

177 differences are not meaningful. The most severe mutation, LasR S129M responded
178 exclusively to $3OC_{12}HSL$ but it was the least sensitive of all the mutants to this ligand.
179 Conversely, among the mutants, LasR S129C responded to the largest range of HSL
180 varieties and it was the most sensitive. In Figure 3A, we provide the assay results for
181 LasR S129F with the five test HSLs. We chose LasR S129F as the representative mutant
182 for in-depth analysis because it had intermediate EC_{50} values among those obtained for
183 this set of mutants. We assayed LasR S129F at 10 μM of each compound, because
184 increased ligand concentration was required to activate LasR S129F compared to
185 wildtype LasR (see Table 1 and Figure 1). At 10 μM ligand, wildtype LasR and LasR
186 S129F maximally responded to $3OC_{12}HSL$ and $3OC_{14}HSL$. However, compared to
187 wildtype LasR, LasR S129F was 7-fold less responsive to $3OC_{10}HSL$, 13-fold less
188 responsive to $3OC_{6}HSL$ and showed almost no response to $3OC_{8}HSL$. In the Δ*lasI P.*
189 *aeruginosa* strain (Figure 3B), LasR S129F displayed a similar pattern. Together, our data
190 indicate that alteration of LasR S129 restricts the set of HSLs that can activate LasR but
191 also increases the EC_{50} values of activating HSLs. We conclude that LasR S129 drives
192 selectivity. While the LasR S129 variants improve selectivity, they diminish sensitivity.
193 This finding suggests that a trade-off exists between selectivity and EC_{50}.
194
195 <u>LasR L130F drives ligand sensitivity</u>
196 Because LasR S129F improves ligand selectivity and reduces sensitivity, we
197 suspected that other residues in the vicinity could also affect ligand selectivity. For this
198 reason, we exchanged L128 and L130 for phenylalanine. As above, we tested their

199 responses to the set of representative HSLs using the *E. coli* p*lasB-lux* reporter assay.
200 Table 1 shows that, surprisingly, LasR L130F exhibited a lower EC_{50} for every autoinducer
201 tested. LasR L128F also conferred improved sensitivity to some short chain HSLs (Table
202 S1), but its phenotype was less pronounced than that of LasR L130F, so we further
203 analyzed the LasR L130F mutant here. Figure 3C shows the wildtype LasR and the LasR
204 L130F responses to a low concentration (50 nM) of the test HSLs. At this concentration,
205 LasR L130F was roughly equivalent to wildtype LasR with respect to the response to
206 $3OC_{12}HSL$, $3OC_{14}HSL$, and $3OC_{10}HSL$. However, LasR L130F was approximately 5-fold
207 more responsive to $3OC_8HSL$ than wildtype LasR and it was modestly more responsive
208 to $3OC_6HSL$. When we performed the *P. aeruginosa* elastase assay at 50 nM test
209 compound (Figure 3D), wildtype LasR only responded to $3OC_{12}HSL$, whereas LasR
210 L130F responded to $3OC_{14}HSL$, $3OC_{10}HSL$, and $3OC_8HSL$ in addition to $3OC_{12}HSL$.
211 Collectively, these results show that LasR L130F is more sensitive to HSLs than wildtype
212 LasR but it is less selective.

213 We used thermal shift analyses to explore the mechanism underlying the
214 increased sensitivity of the LasR L130F mutant for HSLs. We used $3OC_{12}HSL$ and
215 $3OC_{14}HSL$ as our test ligands. Compared to the wildtype LasR LBD, the LasR LBD L130F
216 is more stable when bound to each ligand (Figure 4A), suggesting that the L130F
217 alteration increases the overall stability of the LasR protein. We exploited this feature to
218 successfully purify the LasR LBD L130F bound to $3OC_8HSL$. As mentioned above, we
219 could not purify the wildtype LasR LBD bound to $3OC_8HSL$. We performed thermal shift
220 analyses on the LasR LBD L130F bound to $3OC_8HSL$, $3OC_{10}HSL$, $3OC_{12}HSL$, and

221 $3OC_{14}HSL$ to which we added different HSLs. Similar to the wildtype LasR LBD,
222 exogenous addition of HSLs with long acyl chains further enhanced the stability of the
223 LasR LBD L130F:HSL complexes compared to when HSLs with shorter acyl chains were
224 added (Figure 2 and Figure 4B). For instance, the LasR LBD L130F:$3OC_8HSL$ stability
225 was enhanced by the addition of $3OC_8HSL$, $3OC_{10}HSL$, $3OC_{12}HSL$, and $3OC_{14}HSL$ but
226 not $3OC_6HSL$ (Figure 4B). Protein solubility analyses track with these findings; long acyl
227 chain ligands solubilize the LasR LBD L130F protein whereas short chain ligands do not
228 (Figure 4C, Figure S1B). Consistent with our EC_{50} values, chain length appears to be the
229 most important factor driving protein solubility and stabilization for both the LasR LBD and
230 the LasR LBD L130F (Figure S1B and Figure 4B, respectively).
231
232 <u>LasR ligand selectivity and sensitivity influence the timing of quorum-sensing-controlled</u>
233 <u>traits</u>
234 We have shown that LasR L130F detects and responds to HSLs at lower
235 concentrations than does wildtype LasR, whereas LasR S129F requires higher
236 concentrations. Thus, we predicted that introducing these alleles into *P. aeruginosa*
237 should influence its quorum-sensing responses in opposing manners. To test this
238 prediction, we assayed pyocyanin production over time as the quorum-sensing readout
239 in response to $3OC_{12}HSL$, $3OC_{14}HSL$, and $3OC_8HSL$ in a Δ*lasI P. aeruginosa* strain
240 containing wildtype *lasR*, *lasR S129F*, or *lasR L130F*. Guided by the EC_{50} values for each
241 HSL, we tested appropriate low and high concentrations of each HSL to set windows that
242 would enable us to observe responses from the wildtype and each mutant. Consistent

243 with their relative EC_{50} values, when a low concentration of $3OC_{12}HSL$ (50 nM) was
244 added, the strain with LasR L130F made more pyocyanin than the strain with wildtype
245 LasR at every time point (Figure 5A). At this HSL concentration, the strain carrying LasR
246 S129F never activated pyocyanin production, presumably because the concentration of
247 $3OC_{12}HSL$ was far below the EC_{50} for LasR S129F (Figure 5A). When the same assay
248 was performed with 1μM $3OC_{12}HSL$, rapid and maximal pyocyanin output occurred for *P.*
249 *aeruginosa* carrying both wildtype LasR and LasR L130F. Furthermore, this high ligand
250 concentration reveals that LasR S129F can drive pyocyanin production in response to
251 $3OC_{12}HSL$, albeit weakly and only after 5.5 hours (Figure 5B). A similar pattern was
252 observed for the low concentration of $3OC_{14}HSL$. Specifically, LasR L130F activated
253 pyocyanin production earlier than wildtype LasR, and LasR S129F failed to activate
254 pyocyanin production (Figure 5C). At the high concentration of $3OC_{14}HSL$, LasR S129F
255 did activate pyocyanin production, however later and less strongly than wildtype LasR
256 and LasR L130F (Figure 5D). With respect to $3OC_8HSL$, at both low and high
257 concentrations, all of the responses were considerably weaker than with the longer chain
258 HSLs, nonetheless, in each case, LasR L130F more strongly activated pyocyanin
259 production than wildtype LasR (Figure 5E, F). LasR S129F showed no response in the
260 $3OC_8HSL$ assays (Figure 5E, F).

261 We note one curious finding with 10 μM $3OC_{14}HSL$ in Figure 5D. At this
262 concentration, wildtype LasR activated pyocyanin earlier and more strongly than LasR
263 L130F, which does not track with the EC_{50} values and all of our above companion
264 analyses. We propose that this phenotype is due to RsaL accumulation. RsaL is a

265 quorum-sensing regulator whose expression is activated by LasR (Rampioni et al., 2007;
266 Schuster & Greenberg, 2007). RsaL represses pyocyanin production genes (Cabeen,
267 2014; Schuster & Greenberg, 2007). We propose that because LasR L130F is more
268 active than wildtype LasR, at high autoinducer concentration, LasR L130F possesses
269 increased activity relative to wildtype LasR, and so LasR L130F stimulates higher RsaL
270 production than does wildtype LasR. As a consequence, partial pyocyanin inhibition
271 occurs. This logic suggests that, at high autoinducer concentration, wildtype LasR would
272 activate sufficient RsaL production to cause pyocyanin inhibition. Indeed, addition of 100
273 μM $3OC_{12}HSL$ to the Δ*lasI* strain carrying wildtype LasR induced less pyocyanin
274 production than when 1 μM $3OC_{12}HSL$ was added (Figure S2). We show that RsaL is
275 responsible for this phenotype by deleting the *rsaL* gene. As expected, the Δ*lasI* Δ*rsaL*
276 strain produced increased overall pyocyanin relative to the Δ*lasI* strain. Importantly,
277 however, unlike the Δ*lasI* strain, the Δ*lasI* Δ*rsaL* double mutant does not produce more
278 pyocyanin in response to 1 μM $3OC_{12}HSL$ than in response to 100 μM $3OC_{12}HSL$ (Figure
279 S2). We never observed pyocyanin reductions in the strains carrying any of the LasR
280 alleles when $3OC_8HSL$ was added, even at 100 μM. We suspect this is because
281 $3OC_8HSL$ is such a poor agonist that there is not enough LasR activity at any
282 concentration to stimulate high level RsaL accumulation.
283
284 <u>Structural basis underlying LasR ligand preferences</u>
285 To determine the molecular basis enabling LasR to accommodate non-native
286 autoinducers, we determined the structures of the LasR LBD L130F bound to $3OC_{10}HSL$

287 and $3OC_{14}HSL$. As mentioned, the wildtype LasR LBD structure bound to the native
288 autoinducer, $3OC_{12}HSL$ already exists (Bottomley et al., 2007). Our rationale for using
289 the LasR LBD L130F mutant for these studies was that, its inherently enhanced stability,
290 as judged by the thermal shift data (Figure 4A), suggested that it would be ideal for
291 crystallographic studies that are not possible with the wildtype LasR LBD. Indeed, we
292 could determine the structures of LasR LBD L130F:$3OC_{10}HSL$ and LasR LBD
293 L130F:$3OC_{14}HSL$ to 2.1 Å and 1.9 Å, respectively (Table A1). This resolution is sufficient
294 to observe ligand occupancy and to compare with the LasR LBD:$3OC_{12}HSL$ structure
295 (Figure 6A). The L130F residue is buried in a hydrophobic pocket distal to the ligand
296 binding pocket (Figure S3A). Phenylalanine, rather than leucine at this position, provides
297 increased hydrophobic interactions with amino acid residues L23, L30, F32, I35, L114,
298 L118, L128, L151, and L154. We suggest that this arrangement increases the overall
299 stability of the LasR protein, which in turn, allows it to accommodate an expanded set of
300 HSLs compared to wildtype LasR.

301 To understand how LasR can accommodate multiple long chain HSL ligands in its
302 binding site, we used the crystal structures to examine the key residues and regions of
303 the binding pocket that interact with the different ligands. In all the structures, the lactone
304 head groups have the exact same placement, likely due to strong hydrogen bonding
305 between the lactone ring carbonyl moiety and residue W60 (Figure 6B, displayed in
306 brown). The lactone head group and the ketone moiety on carbon 3 are further stabilized
307 by an extensive hydrogen bonding network comprised of residues Y56, K61, D73, T75,
308 W88, Y93, S129, and S131 (Figure 6B, displayed in brown). In the three structures, the

309 C_{10}, C_{12}, and C_{14} tails take similar paths, until carbon 6, where C_{10} and C_{14} diverge from
310 the path taken by the C_{12} tail in the original structure. Remarkably, this departure in tail
311 path enables both the shorter and longer tails to occupy a similar hydrodynamic volume
312 as the tail on 3OC$_{12}$HSL (Figure S3B). The volume constraint is likely established by
313 hydrophobic interactions with residues G38, L40, A50, I52, A70, V76, L125, and A127
314 (Figure 6B, displayed in pink). These same residues are also responsible for stabilizing
315 3OC$_{10}$HSL in the ligand binding pocket. However, because the C_{10} tail is two carbons
316 shorter than that of the native ligand, the terminal carbons in 3OC$_{10}$HSL have higher
317 intrinsic flexibility at the ligand-protein interface. The measured B-factors suggest
318 increased flexibility stems from less stable hydrophobic interactions (Figure 6C).

319 We next investigated whether there were any structural rearrangements in the
320 crystals that could account for the expanded HSL binding capabilities of LasR L130F
321 compared to wildtype LasR. An ~2 Å shift occurs in the loop corresponding to residues
322 40-52 (highlighted by asterisks in Figure 6A) in the LasR LBD L130F:3OC$_{14}$HSL structure
323 compared to the LasR LBD L130F protein complexed with 3OC$_{10}$HSL and the wildtype
324 LasR LBD complexed with 3OC$_{12}$HSL (Figure 6A and 6C). This loop corresponds to a
325 region with above average B-factor, as depicted by magenta coloring in Figure 6C. The
326 alteration in the positioning of the loop indicates that it could be important for
327 accommodating different HSLs. To test this possibility, we mutated LasR residue Y47 in
328 this loop. We chose Y47 because it is the residue that shifts the most among the different
329 structures. LasR Y47S and LasR Y47R displayed decreased sensitivity to both 3OC$_{12}$HSL
330 and 3OC$_{14}$HSL in the *E. coli* reporter assay (Figure S4) suggesting that the loop provides

331 interactions with the ligand tails that foster increased protein stability, allowing LasR to be
332 activated.

333 To understand the structural basis underlying specificity and promiscuity in this
334 family of proteins, we compared the structures of SdiA LBD:3OC$_8$HSL, CviR LBD:C$_6$HSL,
335 and TraR LBD:3OC$_8$HSL to LasR LBD L130F:3OC$_{14}$HSL (Figure 7A). We chose these
336 particular structures because the receptors display a range of ligand selection
337 preferences – from strict to promiscuous. Similar to what we show here for LasR, SdiA is
338 promiscuous with respect to ligand selectivity (Michael et al., 2001; Nguyen et al., 2015;
339 Sitnikov et al., 1996). Conversely, CviR and TraR display strict specificity for their native
340 autoinducers (Chen et al., 2011; Vannini et al., 2002; Zhang et al., 2002; Zhu & Winans,
341 2001). In terms of overall tertiary structure, a loop similar to the one we pinpoint in Figure
342 6A as critical for LasR to accommodate different ligands, exists in the SdiA LBD (Figure
343 7A). No such loop exists in the CviR and TraR LBD structures (Figure 7A). This result is
344 consistent with the idea that this flexible loop confers ligand promiscuity.

345 In addition to the differences in the overall structures of the receptors, we noted
346 different conformations for the acyl chains in the LasR LBD structures compared to those
347 in the other LuxR-type receptors. The autoinducer acyl chains in the CviR, TraR, and
348 SdiA LBD structures have similar conformations within the ligand binding pockets
349 terminating between residues Y88 and M89 for CviR, Y61 and F62 for TraR, and Y71 and
350 Q72 for SdiA. By contrast, the acyl chains of the different ligands in the LasR LBD L130F
351 structures orient their terminal carbons toward the opposing face of the ligand binding
352 pocket (Figure 7B). These different paths appear to be driven by the hydrophobic

353 interactions we described above for the different LasR ligands (Figure 6B). We identified
354 eight hydrophobic residues (G38, L40, A50, I52, A70, V76, L126, and A127) that dictate
355 the shape of the ligand binding pocket in LasR. Indeed, these residues have generally
356 hydrophobic characteristics in all LuxR-type proteins, but the size of each sidechain varies
357 (Figure 7B). For example, A127 in LasR corresponds to F132 in SdiA. The smaller residue
358 in LasR accommodates the altered path taken by its autoinducer, allowing the terminal
359 carbon of the acyl chain to bind proximal to residue A127. A bulkier residue at this
360 position, as in SdiA, sterically hinders this path for the ligand, forcing the acyl chain to
361 bend in the opposite direction. Thus, in SdiA, F132 forces the terminal carbon of
362 3OC$_8$HSL to bind distally. Indeed, the I153 residue in CviR and the M127 residue in TraR
363 appear to perform roles analogous to F132 in SdiA in dictating the distal orientations of
364 their ligands.

365 Our crystal structures suggest that LasR G38 could also be important for allowing
366 HSL tails to adopt a conformation different from those in SdiA, TraR, and CviR and, in so
367 doing, possibly affect LasR ligand selection (Figure 7B). SdiA, TraR, and CviR all contain
368 larger amino acid sidechains (C45, L45, and A59, respectively) at this position (Figure
369 7B). LasR G38 lies proximal to carbons 9 and 10 in the acyl chains of all the ligands in all
370 the LasR LBD structures. Presumably, a bulkier side chain would sterically hinder the
371 preferred tail paths for 3OC$_{12}$HSL or 3OC$_{14}$HSL, but might enhance the binding of short
372 chain HSLs, such as 3OC$_6$HSL, due to increased hydrophobic interactions. To test this
373 prediction, we mutated G38 in LasR to bulkier amino acids: leucine, isoleucine, and
374 alanine. We tested these alleles in our *E. coli* p*lasB-lux* reporter in response to both a

375 short ($3OC_6HSL$) and a long ($3OC_{12}HSL$) chain HSL (Figure 7C). LasR G38I produced
376 low p*lasB-lux* activity with both molecules suggesting that isoleucine is too bulky to
377 accommodate any HSL well. Consistent with this interpretation, the EC_{50} values for LasR
378 G38I were 533 nM for $3OC_{12}HSL$ and ~66 μM for $3OC_6HSL$. By contrast, LasR G38A and
379 LasR G38L fully activated the reporter in response to both test ligands (Figure 7C). The
380 EC_{50} values for wildtype LasR, LasR G38A, LasR G38L, and LasR L130F were equivalent
381 for $3OC_{12}HSL$ (2.8 nM, 2.5 nM, 2.3 nM, and 2.0 nM, respectively, Figure 7C, top panel).
382 However, the EC_{50} values for LasR G38A and LasR G38L were lower (1.3 μM and 1.6
383 μM, respectively) than that of wildtype LasR (2.4 μM) for $3OC_6HSL$ (Figure 7C, bottom
384 panel). These values are comparable to that of LasR L130F for $3OC_6HSL$ (1.4 μM, Figure
385 7C, bottom panel). Given that we have established that LasR L130F is more stable than
386 wildtype LasR, irrespective of ligand chain length, we suggest that the findings in Figure
387 7 support the hypothesis that larger amino acid residues at G38 improve the LasR affinity
388 for shorter chain HSLs by forming more stable protein-ligand complexes.
389

390 **Discussion**

391 *P. aeruginosa* can live in environments in which it encounters other bacterial
392 species that produce HSL autoinducers (Tashiro, Yawata, Toyofuku, Uchiyama, &
393 Nomura, 2013). Our results show that LasR can, with reduced affinity, detect non-native
394 HSLs and in response, activate transcription of quorum-sensing target genes. We
395 suggest that determining the mechanisms that promote or restrict ligand access to LasR
396 is important for understanding how the *P. aeruginosa* quorum-sensing response could be

397 naturally or synthetically manipulated. Here, we identified mutations that alter the
398 selectivity and sensitivity of LasR. We found that LasR L130F improves LasR sensitivity,
399 but at the cost of decreased selectivity. In contrast, we find that alterations at LasR S129
400 can increase selectivity for autoinducer recognition but, that feature is offset by a
401 reduction in sensitivity. Our findings suggest that LasR balances ligand sensitivity with
402 selectivity. The LasR S129 mutants show that decreasing the LasR sensitivity to ligands
403 dampens and delays the quorum-sensing response (Figure 3B and Figure 5). We
404 presume that inadequate activation decreases the potency of *P. aeruginosa* virulence. By
405 contrast, the more sensitive LasR L130F allele causes higher and premature activation
406 of quorum sensing (Figure 3D and Figure 5). In this case, the release of expensive public
407 goods before the population is at a sufficient cell density to optimally use those goods
408 could promote cheating. LasR L130F may also negatively influence virulence at high
409 autoinducer concentration by stimulating overproduction of RsaL (Figure 5D).

410 We investigated the published sequences of hundreds of clinical isolates of *P.*
411 *aeruginosa* and we did not find any strain that possessed a mutation at either S129 or
412 L130 (Feltner et al., 2016). We conclude that it is detrimental for LasR to become either
413 more sensitive to or less selective for ligands. Perhaps, striking the ideal balance between
414 selectivity and sensitivity in LasR means that detection of some non-native HSLs must be
415 tolerated, although, importantly, only at higher concentrations relative to the native
416 autoinducer.

417 We propose that LasR promiscuity could serve an important function in the
418 environment (i.e., soil) and in eukaryotic hosts where *P. aeruginosa* encounters other

419 species of bacteria. We suggest that LasR detection of non-native HSLs enables it to
420 "eavesdrop" on its competitors. However, our finding that 3OC$_{12}$HSL is the most potent
421 agonist indicates that *P. aeruginosa* prioritizes detecting its own autoinducer over those
422 of other species. Amongst our set of test compounds, 3OC$_{14}$HSL is the second best LasR
423 agonist and it is also highly potent, indicating that the LasR receptor has not optimized
424 against detection of longer chain HSLs. Possibly, *P. aeruginosa* readily interacts with
425 3OC$_{14}$HSL-producing bacteria. Alternatively, *P. aeruginosa* might not encounter
426 3OC$_{14}$HSL in its natural surroundings as, presently, scant evidence exists for natural
427 production of 3OC$_{14}$HSL by bacteria. There are two preliminary reports of soil-dwelling
428 nitrogen-fixing bacteria that are capable of making 3OC$_{14}$HSL, 3OHC$_{14}$HSL and/or
429 C$_{14}$HSL (Gao, Ma, Zhuang, & Zhuang, 2014; Mellbye, Spieck, Bottomley, & Sayavedra-
430 Soto, 2017), but if, when, and how much they do remains mysterious. Specifically, mass
431 spectrometry and bioassay show that *Nitrosospira briensis* produces 3OHC$_{14}$HSL, but
432 only at concentrations of 1 nM (Mellbye et al., 2017), too low for detection by wildtype
433 LasR. Second, *Nitrospira multiformis* has a LuxI-type synthase (NmuI) that produces
434 3OC$_{14}$HSL and C$_{14}$HSL in recombinant *E. coli*. However, neither of these molecules
435 solubilized the putative receptor, NmuR, and no conditions were identified under which
436 *Nitrospira multiformis* produced the molecules (Gao et al., 2014). Future study will be
437 necessary to determine the prevalence of HSLs longer than C$_{12}$ in nature and whether *P.*
438 *aeruginosa* encounters such molecules.

439 With the one exception of 3OC$_{14}$HSL, wildtype LasR detects 3OC$_{12}$HSL far more
440 efficiently than other HSLs. Therefore, it is likely that, in mixed-species consortia,

441 3OC$_{12}$HSL out-competes all other autoinducers. This finding suggests that while LasR is
442 capable of detecting non-cognate autoinducers, it does not do so when *P. aeruginosa* is
443 the majority species. However, we propose that there could exist conditions under which
444 low-affinity "eavesdropping" would benefit *P. aeruginosa.* First, when *P. aeruginosa* is at
445 low cell density, provision of non-cognate ligands made by other bacterial species that
446 are at higher cell density could induce *P. aeruginosa* to activate its quorum-sensing
447 behaviors prematurely relative to when it is at low cell density in mono-species culture. If
448 so, *P. aeruginosa* could synthesize toxic defensive products such as pyocyanin and
449 rhamnolipids that endow it with an advantage over competing species (Baron & Rowe,
450 1981; Smalley, An, Parsek, Chandler, & Dandekar, 2015). Beyond defensive products,
451 perhaps some of the quorum-sensing-controlled products produced under such
452 conditions can be used exclusively by *P. aeruginosa* and not by competing species. If so,
453 LasR promiscuity could grant *P. aeruginosa* a "last ditch" opportunity to survive in
454 environments in which it is vastly outnumbered by competing species.

455 Our combined genetic, biochemical, and structural work revealed the molecular
456 basis for non-native autoinducer recognition by LasR. There exists a key flexible loop
457 that, if present (LasR, SdiA), endows particular LuxR-type receptors with the ability to
458 bind to multiple HSL ligands, but if absent (TraR, CviR), the LuxR-type receptor is highly
459 specific for a particular HSL ligand. Indeed, this structure-function analysis could explain
460 why a competitive inhibitor of CviR, chlorolactone (CL), behaves as an agonist in *P.*
461 *aeruginosa* (O'Loughlin et al., 2013). These findings are particularly enlightening when
462 considering attempts to design inhibitors that specifically target different LuxR-type

463 receptors. The flexible loop and hydrophobic residues in LasR near the acyl chain binding
464 site that we pinpoint here will need to be taken into account when developing small
465 molecule inhibitors that target LasR or other LuxR-type proteins that possess this feature.
466 Designing molecules that target the flexibility of the loop region and/or that destabilize the
467 protein could be explored for promiscuous receptors, such as LasR. By contrast, targeted
468 screening around molecules that resemble CL could yield inhibitors for LuxR-type
469 proteins that display strict specificity for their cognate autoinducers, such as CviR.
470

471 **Materials and Methods**

472 Site directed mutagenesis:

473 Mutations in *lasR* were constructed on the pBAD-A-*lasR* plasmid (Paczkowski et al.,
474 2017). Primers were designed using the Agilent Quikchange primer design tool and PCR
475 with pFUltra polymerase (Agilent). PCR reactions were treated with DpnI to eliminate
476 parental plasmid DNA and the plasmids with the mutant *lasR* genes were transformed
477 into One Shot TOP10 chemically competent *E. coli* cells (Invitrogen). Reactions were
478 plated on LB agar plates containing ampicillin (50 μg/mL) and individual mutants were
479 verified via sequencing with primers for the *lasR* gene (ARM203 and ARM204). Primers
480 and strains used in this work are listed in Table A2 and Table A3, respectively.
481

482 *P. aeruginosa* strain construction:

483 In-frame, marker-less *lasR* mutations were engineered onto the chromosome of *P.*
484 *aeruginosa* PA14 using pEXG2-suicide constructs with gentamicin selection and *sacB*

485 counter selection (Borlee, Geske, Blackwell, & Handelsman, 2010; Kukavica-Ibrulj et al.,
486 2008). The *lasR* gene and 500 bp of flanking regions were cloned into pUCP18
487 (Schweizer, 1991). Site directed mutagenesis was performed as described above to
488 construct point mutations in plasmid-borne *lasR*. The DNA carrying the mutant *lasR*
489 genes was obtained from pUCP18 by restriction enzyme digestion with BamHI and EcoRI
490 (NEB), and subsequently, the fragments were ligated into pEXG2. The recombinant
491 pEXG2 plasmids were transformed into *E. coli* SM10λ*pir* and, from there, the plasmids
492 were mobilized into *P. aeruginosa* PA14 via biparental mating (Mukherjee, Moustafa,
493 Smith, Goldberg, & Bassler, 2017; Simon, Priefer, & Puhler, 1983). Exconjugants were
494 selected on LB plates containing 30 μg/mL gentamicin and 100 μg/mL irgasan after
495 overnight growth at 37° C. After recovery, 5% sucrose was used to select for loss of the
496 plasmid. Candidate mutants were patched onto LB plates and LB plates containing 30
497 μg/mL gentamicin to select against the resistance marker. Colony PCR was performed
498 on gentamicin sensitive patches with primers that annealed 500 bp [base pairs] upstream
499 and downstream of *lasR* (ARM455 and ARM456). These PCR products were sequenced
500 with *lasR* forward and reverse primers (ARM203 and ARM204).
501
502 <u>*E. coli* p*lasB-lux* reporter assay for LasR activity</u>:
503 The development of an assay that reports on LasR activity in response to exogenous
504 ligands using luciferase as the readout has been described previously (Paczkowski et al.,
505 2017). In brief, 2 μL of overnight cultures containing p*lasB-luxCDABE* and pBAD-A with
506 either wildtype *lasR* or mutant *lasR* alleles were back diluted into 200 μL LB medium and

507 placed into clear-bottom 96-well plates (Corning). The plates were shaken at 30° C for 4
508 h and 0.1% arabinose was added to each well along with a test HSL at the concentrations
509 designated in the text and figures. To perform dose response analyses, 1 mM of each
510 HSL was serially diluted 3-fold 10 times, and 2 μL of each dilution was added to the wells.
511 Higher or lower HSL concentrations were assayed when EC_{50} values did not fall into this
512 range. Plates were shaken at 30° C for 4 h. Bioluminescence and OD_{600} were measured
513 using a Perkin Elmer Envision Multimode plate reader. Relative light units were calculated
514 by dividing the bioluminescence measurement by the OD_{600} nm measurement. Non-linear
515 regression was performed in Graphpad Prism6 to obtain EC_{50} values.
516
517 Elastase assay:
518 The *P. aeruginosa* PA14 Δ*lasI* strains carrying either wildtype or mutant *lasR* genes were
519 grown overnight with shaking at 37° C in LB medium. Cultures were back diluted 1:50 in
520 3 mL of LB and grown for an additional 8 h with shaking at 37° C. Strains were back
521 diluted 1:1000 into 3 mL of LB medium and test HSLs or an equivalent volume of DMSO
522 were added to each culture. These cultures were grown overnight at 37° C with shaking.
523 1 mL of each culture was removed and the cells were pelleted by centrifugation at 16,100
524 x g. The supernatant was removed and filtered through a .22 μm filter (Millipore) and 100
525 μL of supernatant was added to 900 μL of 10 mM Na_2HPO_4 containing 10 mg of elastin-
526 Congo red substrate (Sigma-Aldrich). These preparations were incubated at 37° C for 2
527 h. The mixtures were subjected to centrifugation at 16,100 x g for 10 min. The resulting

528 supernatants were removed and OD_{495} nm measured with a Beckman Coulter DU730
529 spectrophotometer against a blank of H_2O.
530
531 Thermal shift assay:
532 Thermal shift analyses of 6xHis-LasR LBD and 6xHisLasR L130F LBD bound to HSLs
533 were performed as previously described (Paczkowski et al., 2017). In short, ligand-bound
534 protein was diluted to 5 μM in reaction buffer (20 mM Tris-HCL pH 8, 200 mM NaCl, and
535 1 mM DTT [dithiothreitol]) containing DMSO or 10 μM HSL test compound in 18 μL total
536 volume. The mixtures were incubated at room temperature for 15 min. 5000x SYPRO
537 Orange (Thermo-Fisher) in DMSO was diluted to 200x in reaction buffer and used at 20x
538 final concentration. 2 μL of 200x SYPRO Orange was added to the 18 μL sample
539 immediately prior to analysis. Samples were subjected to a linear heat gradient of 0.05
540 ^{o}C/s, from 25 ^{o}C to 99 ^{o}C in a Quant Studio 6 Flex System (Applied Biosystems) using
541 the melting curve setting. Fluorescence was measured using the ROX reporter setting.
542
543 Pyocyanin time course:
544 Overnight cultures of the *P. aeruginosa* Δ*lasI*, Δ*lasI lasR S129F*, Δ*lasI lasR L130F*, and
545 Δ*lasI* Δ*rsaL* strains were grown in LB medium with shaking at 37° C. 1.5 mL of each
546 culture was diluted into 50 mL of fresh LB medium. HSLs were added at the
547 concentrations described in the text and figures and the cultures were shaken at 37° C
548 for an additional 3 h. From there forward, 1 mL aliquots were removed every 30 min for
549 300 min and cell density (OD_{600} nm) was measured immediately using a Beckman Coulter

550 DU730 Spectrophotometer. The aliquots were subjected to centrifugation at 16,100 x g
551 for 2 min and the clarified supernatants were removed. The OD_{695} nm of the supernatants
552 were measured. Pyocyanin activity was determined by plotting the OD_{695} nm/OD_{600} nm
553 over time for each strain.
554
555 Protein production, purification, and crystallography:
556 Recombinant 6xHis-LasR LBD and 6xHis-LasR LBD L130F proteins bound to $3OC_8HSL$,
557 $3OC_{10}HSL$, $3OC_{12}HSL$, or $3OC_{14}HSL$ were purified as previously described for LasR
558 LBD:$3OC_{12}HSL$ using Ni-NTA affinity columns followed by size exclusion
559 chromatography (Paczkowski et al., 2017). 6xHis-LasR LBD bound to $3OC_{10}HSL$ and
560 6xHis-LasR LBD bound to $3OC_{14}HSL$ were crystallized by the hanging drop diffusion
561 method. Diffraction data were processed using the HKL-3000 software package (Minor,
562 Cymborowski, Otwinowski, & Chruszcz, 2006). The structures were solved using Phaser
563 in Phenix (Adams et al., 2011; Afonine et al., 2012) by molecular replacement, with the
564 structure of LasR LBD:$3OC_{12}HSL$ used as the search model (Bottomley et al., 2007).
565 Model building was performed using Coot (Emsley & Cowtan, 2004; Emsley, Lohkamp,
566 Scott, & Cowtan, 2010) and further refinement was accomplished using Phenix (Adams
567 et al., 2011). Images of the structures were generated with PyMOL (DeLano, 2009). When
568 we describe specific amino acid or amino acid-ligand interactions, we provide the image
569 for the best resolved example in the asymmetric unit.
570
571 Protein solubility assay:

572 *E. coli* BL21 DE3 (Invitrogen) containing plasmid-borne 6xHis-LasR LBD or 6xHis-LasR
573 LBD L130F were grown overnight and back diluted 1:500 in 20 mL of LB medium
574 containing ampicillin (100 μg/mL). Cultures were grown to OD_{600} of 0.5 and protein
575 production was induced with 1 mM IPTG [Isopropyl β-D-1-thiogalactopyranoside]. Upon
576 addition of IPTG, the desired test HSL was also added at a final concentration of 10 μM,
577 and the cultures were incubated at 25 ^{o}C with shaking for 4 h. Cells were harvested at
578 3,000 x g and resuspended in lysis buffer (500 mM NaCl, 20 mM Tris-HCL pH 8, 20 mM
579 imidazole, 5% glycerol, 1 mM EDTA, and 1 mM DTT). The cells were lysed using
580 sonication (1 s pulses for 15 s with a 50% duty cycle). The fraction we call the whole cell
581 lysate was harvested after sonication. The soluble fraction was isolated by centrifugation
582 at 32,000 x g. Samples were subjected to electrophoresis on SDS-PAGE gels (Biorad)
583 and imaged with an Image Quant LAS4000 gel dock using the trans-illumination setting
584 (GE Healthcare).
585
586 <u>Homoserine lactone synthesis:</u>
587 Unless otherwise indicated, all temperatures are expressed in °C (degrees Centigrade).
588 All reactions were conducted at room temperature unless otherwise noted. ^{1}H-NMR
589 spectra were recorded on a Varian VXR-400, or a Varian Unity-400 at 400MHz
590 [megahertz] field strength. Chemical shifts are expressed in parts per million (ppm, δ
591 units). Coupling constants (*J*) are in units of hertz (Hz). Splitting patterns describe
592 apparent multiplicities and are designated as s (singlet), d (doublet), t (triplet), q (quartet),
593 m (multiplet), quin (quintet) or br (broad). Mass spectrometry analyses were performed

594 on a Sciex API 100 using electrospray ionization (ESI). LCMS was carried out using a C-
595 18 reverse phase column (2.1 ID, 3.5 micron, 50 mm). The column conditions were 98%
596 water with 0.05%TFA and 2% MeOH [methanol] to 100% MeOH over 5.5 min. Analytical
597 thin layer chromatography was used to verify the purity as well as to follow the progress
598 of reaction(s). Unless otherwise indicated, all final products were at least 95% pure as
599 judged by HPLC / MS. Synthesis is diagrammed in Appendix Figure 1.
600
601 General procedure for the synthesis of homoserine lactones. To a solution of (3*S*)-3-
602 aminotetrahydrofuran-2-one (1.00 eq, HBr salt) and Et_3N (3.00 eq) in DCM was added a
603 solution of the acid chloride (1.00 eq) in DCM. The resulting reaction mixture was stirred
604 at room temperature for 3 h. The reaction mixture was then diluted with H_2O (5 mL), and
605 extracted with DCM (3 x 5 mL). The organic layers were combined, washed with brine
606 (10 mL), dried over Na_2SO_4, filtered, and concentrated under reduced pressure to give a
607 residue. The residue was purified by silica gel column chromatography to give the desired
608 homoserine lactone as a white solid.
609
610 (*S*)-*N*-(2-oxotetrahydrofuran-3-yl)hexanamide (BB0189). Gradient elution with Petroleum
611 ether/EtOAc = 3/1 to 1/1 afforded the title compound (425 mg, 96% yield, 98% purity by
612 LC/MS) as a white solid. ^{1}H NMR ($CDCl_3$) δ = 6.26 (s, 1H), 4.63 (m, 1H), 4.50 (td, *J* = 1.0,
613 5.6, 1H), 4.33 (m, 1H), 2.87 (m, 1H), 2.27 (t, *J* = 7.4, 2H), 2.20 (m, 1H), 1.71 (t, *J* = 7.4,
614 2H), 1.34 (m, 4H), 0.90 (t, *J* = 7.1, 3H); MS (ESI) calculated for $C_{10}H_{17}NO_3$: m/z = 199;
615 found: m/z = 200 (M+H).

616 (S)-*N*-(2-oxotetrahydrofuran-3-yl)octanamide (BB0192). Gradient elution with Petroleum
617 ether/EtOAc = 3/1 to 1/1 afforded the title compound (270 mg, 96% yield, 99% purity by
618 LC/MS) as a white solid. ^{1}H NMR ($CDCl_3$) δ = 5.94 (s, br, 1H), 4.54 (m, 2H), 4.29 (ddd, *J*
619 = 5.9, 9.5, 11.3, 1H), 2.88 (m, 1H), 2.26 (t, *J* = 7.7, 2H), 2.13 (m, 1H), 1.63 (m, 2H), 1.30
620 (m, 8H), 0.89 (t, *J* = 6.6, 3H); MS (ESI) calculated for $C_{12}H_{21}NO_3$: m/z = 227; found: m/z
621 = 228 (M+H).
622
623 (*S*)-*N*-(2-oxotetrahydrofuran-3-yl)decanamide (BB0195). Gradient elution with Petroleum
624 ether/EtOAc = 10/1 to 1/1 afforded the title compound (632 mg, 94% yield, 99% purity by
625 LC/MS) as a white solid. ^{1}H NMR ($CDCl_3$) δ = 6.01 (s, br, 1H), 4.55 (ddd, *J* =5.7, 8.6,
626 11.6, 1H), 4.47 (t, *J* = 9.2, 1H), 4.29 (ddd, *J* = 6.1, 9.4, 11.2, 1H), 2.87 (m, 1H), 2.25 (t, *J*
627 = 7.7, 2H), 2.12 (m, 1H), 1.66 (m, 2H), 1.30 (m, 12H), 0.88 (t, *J* = 6.8, 3H); MS (ESI)
628 calculated for $C_{14}H_{25}NO_3$: m/z = 255; found: m/z = 256 (M+H).
629
630 (*S*)-*N*-(2-oxotetrahydrofuran-3-yl)dodecanamide (BB0198). Gradient elution with
631 Petroleum ether/EtOAc = 10/1 to 1/1 afforded the title compound (632 mg, 94% yield,
632 99% purity by LC/MS) as a white solid. ^{1}H NMR ($CDCl_3$) δ = 5.94 (s, br, 1H), 4.60-4.45
633 (m, 2H), 4.29 (m, 1H), 2.90 (m, 1H), 2.25 (t, *J* = 7.2, 2H), 2.14 (m, 1H), 1.64 (m, 2H), 1.35-
634 1.22 (m, 16H), 0.88 (t, *J* = 6.7, 3H); MS (ESI) calculated for $C_{16}H_{29}NO_3$: m/z = 283; found:
635 m/z = 284 (M+H).
636
637 General Procedures for the synthesis of 3-oxo homoserine lactones.

638 Procedure A: To a stirring solution of 2,2-dimethyl-1,3-dioxane-4,6-dione (Meldrum's
639 acid) (1.00 eq) and DMAP (2.00 eq) in DCM at 0°C was added a solution of the acid
640 chloride (1.00 eq) in DCM. The resulting reaction mixture was allowed to warm to room
641 temperature and stirred for 12 h. The reaction mixture was diluted with DCM (30 mL) and
642 washed with cold 2N HCl (3 x 30 mL). The organic layer was separated, dried over
643 Na_2SO_4, filtered and concentrated under reduced pressure to give a crude product. The
644 crude product was dissolved in anhydrous 1,4 dioxane (5 mL), and then (3*S*)-3-
645 aminotetrahydrofuran-2-one (1.20 eq, HBr salt) and Et_3N (1.00 eq) were added. The
646 resulting reaction mixture was degassed by purging with N_2 3 times, then heated to 100°C
647 for 12 h under an N_2 atmosphere. The reaction mixture was cooled to room temperature,
648 diluted with H_2O (10 mL) and extracted with EtOAc (3 x 10 mL). The combined organic
649 layers were washed with brine (15 mL), dried over Na_2SO_4, filtered, and concentrated
650 under reduced pressure to give a residue. The residue was purified by silica gel column
651 chromatography to give the desired 3-oxo homoserine lactone as a white solid.
652
653 Procedure B: To a stirring solution of 2,2-dimethyl-1,3-dioxane-4,6-dione (Meldrum's
654 acid) (1.00 eq) and DMAP (1.05 eq) in DCM at 0°C was added DCC (1.10 eq) followed
655 by the requisite carboxylic acid (1.00 eq). The resulting reaction mixture was allowed to
656 warm to room temperature and stirred for 12 h. The reaction mixture was filtered through
657 a pad of Celite to remove precipitated solids and concentrated under vacuum. The crude
658 material was diluted with EtOAc (30 mL) and washed with cold 2N HCl (3 x 30 mL). The
659 organic layer was separated, dried over Na_2SO_4, filtered and concentrated under reduced

660 pressure to give a crude product. The crude product was dissolved in anhydrous 1,4
661 dioxane, and then (3*S*)-3-aminotetrahydrofuran-2-one (1.00 eq, HBr salt) and Et_3N (1.00
662 eq) were added. The resulting reaction mixture was degassed by purging with N_2 3 times,
663 then heated to 100°C for 12 h under an N_2 atmosphere. The reaction mixture was cooled
664 to room temperature, diluted with H_2O (10 mL) and extracted with EtOAc (3 x 10 mL). The
665 combined organic layers were washed with brine (15 mL), dried over Na_2SO_4, filtered,
666 and concentrated under reduced pressure to give a residue. The residue was purified by
667 silica gel column chromatography to give the desired 3-oxo homoserine lactone as a white
668 solid.
669
670 (*S*)-3-oxo-*N*-(2-oxotetrahydrofuran-3-yl)hexanamide (BB0187). Following Procedure A,
671 elution with Petroleum ether/EtOAc = 1/1 afforded the title compound (285 mg, 29% yield,
672 97% purity by LC/MS) as a white solid. ^{1}H NMR (400MHz, $CDCl_3$) δ = 1H NMR (300 MHz,
673 CDCl3) δ=7.85 (s, 1H), 4.67 (ddd, *J* = 6.7, 1H), 4.57 (td, *J* = 1.3, 4.2, 1H), 4.34 (m, 1H),
674 3.52 (s, 2H), 2.82 (m, 1H), 2.56 (t, *J* = 7.2, 2H) 2.33 (m, 1H), 1.64 (m, 2H), 0.98 (t, *J* =
675 6.5, 3H); MS (ESI) calculated for $C_{10}H_{15}NO_4$: m/z = 213; found: m/z = 214 (M+H).
676
677 (*S*)-3-oxo-*N*-(2-oxotetrahydrofuran-3-yl)octanamide (BB0190). Following Procedure A,
678 elution with Petroleum ether/EtOAc = 1/1 afforded the title compound (220 mg, 37% yield,
679 99% purity by LC/MS) as a white solid. ^{1}H NMR (400MHz, $CDCl_3$) δ = 7.66 (s, br, 1H),
680 4.60 (m, 1H), 4.48 (t, *J* = 9.0 Hz, 1H), 4.29 (m, 1H), 3.47 (s, 2H), 2.77 (m, 1H), 2.53 (t, *J*

681 = 7.3, 2H), 2.23, m, 1H), 1.61 (m, 2H), 1.31 (m, 4H), 0.90 (t, *J* = 6.6, 3H); MS (ESI)
682 calculated for $C_{12}H_{19}NO_4$: m/z = 241; found: m/z = 242 (M+H).
683
684 (*S*)-3-oxo-*N*-(2-oxotetrahydrofuran-3-yl)decanamide (BB0193). Following Procedure A,
685 gradient elution with Petroleum ether/EtOAc = 10/1 to 2/1 afforded the title compound (75
686 mg, 15% yield, 99% purity by LC/MS) as a white solid. ^{1}H NMR (400MHz, $CDCl_3$) δ =
687 7.68 (s, br, 1H), 4.60 (m, 1H), 4.48 (t, *J* = 9.1, 1H), 4.28 (m, 1H), 3.47 (s, 2H), 2.77 (m,
688 1H), 2.52 (t, *J* = 7.3, 2H), 2.22 (m, 1H), 1.59 (m, 2H), 1.27 (m, 8H), 0.88 (t, *J* = 6.2, 3H);
689 MS (ESI) calculated for $C_{14}H_{23}NO_4$: m/z = 269; found: m/z = 270 (M+H).
690
691 (*S*)-3-oxo-*N*-(2-oxotetrahydrofuran-3-yl)dodecanamide (BB0196). Following Procedure
692 A, gradient elution with Petroleum ether/EtOAc = 5/1 to 2/1 afforded the title compound
693 (940 mg, 56% yield, 99% purity by LC/MS) as a white solid. ^{1}H NMR (400MHz, $CDCl_3$) δ
694 = 7.67 (s, br, 1H), 4.58 (m, 1H), 4.48 (m, 1H), 4.28 (m, 1H), 3.47 (s, 2H), 2.75 (m, 1H),
695 2.52 (t, *J* = 7.3, 2H), 2.22 (m, 1H), 1.59 (m, 2H), 1.27 (m, 12H), 0.88 (t, *J* = 6.2, 3H); MS
696 (ESI) calculated for $C_{16}H_{27}NO_4$: m/z = 297; found: m/z = 298 (M+H).
697
698 (*S*)-3-oxo-*N*-(2-oxotetrahydrofuran-3-yl)tetradecanamide (BB0219). Following Procedure
699 B, gradient elution with Petroleum ether/EtOAc = 20/1 to 1/1 afforded the title compound
700 (3.73 g, 46% yield, 98% purity by LC/MS) as a white solid. ^{1}H NMR (400MHz, $CDCl_3$) δ
701 = 7.67 (d, J = 5.3, 1H), 4.60 (ddd, *J* = 6.8, 8.6, 11.4, 1H), 4.48 (dd, *J* = 9.2, 9.2, 1H), 4.28
702 (ddd, J = 5.9, 9.4, 11.0, 1H), 3.47 (s, 2H), 2.74 (m, 1H), 2.53 (t, *J* = 7.5, 2H), 2.23 (m, 1H),

703 1.59 (m, 2H), 1.26 (m, 16H), 0.91 (t, *J* = 6.8, 3H); MS (ESI) calculated for $C_{18}H_{31}NO_4$:
704 m/z = 325; found: m/z = 326 (M+H).
705
706 General procedure for the synthesis of 3-hydroxy homoserine lactones. To a stirring
707 solution of 3-oxo homoserine lactone (1.00 eq) in DME (3 mL) at 0 °C was added $NaBH_4$
708 (0.35 eq). The resulting reaction mixture was stirred at 0 °C for 2 h. The reaction mixture
709 was concentrated under reduced pressure to give a residue. The residue was purified by
710 silica gel column chromatography to give the desired 3-hydroxy homoserine lactone as a
711 white solid.
712
713 3-hydroxy-*N*-((*S*)-2-oxotetrahydrofuran-3-yl)hexanamide (BB0188). Elution with
714 EtOAc/CH_3CN = 50/1 afforded the title compound (96 mg, 45% yield, 96% purity by
715 LC/MS) as a white solid. ^{1}H NMR (400MHz, $CDCl_3$) δ = 6.64 (dd, br, *J* = 5.2, 20.0, 1H),
716 4.61 (m, 1H), 4.49 (t, *J* = 8.8, 2H), 4.30 (ddd, *J* = 6.0, 9.5, 11.0, 1H), 4.04 (br s, 1H), 3.18
717 (dd, *J* = 3.0, 17.1 Hz, 1H), 2.44 (m, 1H), 2.37 (m, 1H), 2.20(m, 1H), 1.53 - 1.39 (m, 4H),
718 0.94 (t, *J* = 6.8, 3H); MS (ESI) calculated for $C_{10}H_{17}NO_4$: m/z = 215; found: m/z = 216
719 (M+H).
720
721 3-hydroxy-*N*-((*S*)-2-oxotetrahydrofuran-3-yl)octanamide (BB0191). Gradient elution with
722 EtOAc/CH_3CN = 80/1 to 70/1 afforded the title compound (96 mg, 32% yield, 99% purity
723 by LC/MS) as a white solid. ^{1}H NMR (400MHz, DMSO-d_6) δ = 8.31 (s, br, 1H), 4.57 (m,
724 1H), 4.48 (m, 1H), 4.33 (m, 1H), 4.20 (m, 1H), 3.79 (m, 1H), 2.37 (m, 1H), - 2.16 (m, 3H),

725 1.40-1.11 (m, 8H), 0.86 (t, *J* = 6.6, 3H); MS (ESI) calculated for $C_{12}H_{21}NO_4$: m/z = 243;
726 found: m/z = 244 (M+H).
727
728 <u>3-hydroxy-*N*-((*S*)-2-oxotetrahydrofuran-3-yl)decanamide (BB0194).</u> Gradient elution with
729 EtOAc/CH_3CN = 80/1 to 70/1 afforded the title compound (106 mg, 38% yield, 99% purity
730 by LC/MS) as a white solid. ^{1}H NMR (400MHz, $CDCl_3$) δ = 6.63 (d, br, *J* = 20.4, 1H), 4.59
731 (m, 1H), 4.49 (m, 1H), 4.30 (m, 1H), 4.03 (m, 1H), 3.15 (d, br, *J* = 14.0, 1H), 2.81 (m, 1H),
732 2.44 (m, 1H), 2.38 (m, 1H), 2.20 (m, 1H), 1.53 - 1.22 (m, 12H), 0.89 (t, *J* = 6.2, 3H); MS
733 (ESI) calculated for $C_{14}H_{25}NO_4$: m/z = 271; found: m/z = 272 (M+H).
734
735 <u>3-hydroxy-*N*-((*S*)-2-oxotetrahydrofuran-3-yl)dodecanamide (BB0197).</u> Elution with
736 EtOAc/CH_3CN = 100/1 afforded the title compound (137 mg, 47% yield, 99% purity by
737 LC/MS) as a white solid. ^{1}H NMR (400MHz, DMSO-d_6) δ = 8.30 (dd, *J* = 8.1, 11.6, 1H),
738 4.54 (m, 2H), 4.33 (dt, *J* = 1.4, 8.8, 1H), 4.19 (m, 1H), 3.79 (m, 1H), 2.38 (m, 1H), 2.22-
739 2.06 (m, 3H), 1.38-1.18 (m, 16H), 0.86 (t, *J* = 6.7, 3H); MS (ESI) calculated for $C_{16}H_{29}NO_4$:
740 m/z = 299; found: m/z = 300 (M+H).
741
742 <u>Statistical methods:</u>
743 In all experiments, values are the average of 3 biological replicates, each of which was
744 assessed in 2 or 3 technical replicates as noted. For EC_{50} analyses, wildtype LasR was
745 used as the control. EC_{50} values that appear in multiple experiments represent the mean
746 from all experiments (Table 1, Figure 7, Figure S4 and Table S1). In these cases, 3

747 technical replicates of 3 biological replicates were assayed for every protein/molecule in
748 each experiment. Biological replicates are defined as distinct samples analyzed on
749 separate days. Technical replicates are defined as multiple measurements made on the
750 same sample. Error bars represent standard deviations of the means. 2-tailed T-tests
751 were performed to compare experimental groups. P values: *<.05, **<.01, ***<.0001
752

753 **Accession Number**

754 The coordinates and structure factors will be deposited in the Protein Data Bank upon
755 acceptance of the manuscript.
756

757 **Acknowledgements**

758 We thank Dr. Fred Hughson and Dr. Philip Jeffrey for assistance with crystallography. We
759 also thank Dr. Chari Smith and the entire Bassler group for insightful ideas about this
760 research. This work was supported by the Howard Hughes Medical Institute, National
761 Institutes of Health Grant 5R37GM065859, and National Science Foundation Grant MCB
762 1713731 (B.L.B.), NIGMS T32GM007388 (A.R.M), and a Jane Coffin Childs Memorial
763 Fund for Biomedical Research Postdoctoral Fellowship (J.E.P.). The authors declare that
764 they have no conflicts of interest with the contents of this article. The content is solely the
765 responsibility of the authors and does not necessarily represent the official views of the
766 National Institutes of Health.
767

768 **Author Contributions**

769 A.R.M. performed the experiments and interpreted the data in Figures 1, 3, 5, 7, S2, S4
770 and Tables 1 and S1. J.E.P. performed the experiments and interpreted the data in
771 Figures 2, 4, 6, 7, S1, and S3. B.R.H designed the synthesis for all the homoserine
772 lactones used. B.L.B., A.R.M., and J.E.P conceived of the study. B.L.B coordinated the
773 study and helped with interpretation of results. All of the authors contributed to the writing
774 of the manuscript

Literature Cited

Adams, P. D., Afonine, P. V., Bunkóczi, G., Chen, V. B., Echols, N., Headd, J. J., . . . Zwart, P. H. (2011). The Phenix software for automated determination of macromolecular structures. *Methods, 55*(1), 94-106. doi:10.1016/j.ymeth.2011.07.005

Afonine, P. V., Grosse-Kunstleve, R. W., Echols, N., Headd, J. J., Moriarty, N. W., Mustyakimov, M., . . . Adams, P. D. (2012). Towards automated crystallographic structure refinement with phenix.refine. *Acta Crystallogr D Biol Crystallogr, 68*(Pt 4), 352-367. doi:10.1107/S0907444912001308

Albus, A. M., Pesci, E. C., RunyenJanecky, L. J., West, S. E. H., & Iglewski, B. H. (1997). Vfr controls quorum sensing in Pseudomonas aeruginosa. *Journal of Bacteriology, 179*(12), 3928-3935.

Baron, S. S., & Rowe, J. J. (1981). Antibiotic action of pyocyanin. *Antimicrobial Agents and Chemotherapy, 20*(6), 814-820. doi:10.1128/aac.20.6.814

Bassler, B. L., Wright, M., Showalter, R. E., & Silverman, M. R. (1993). Intercellular Signaling in Vibrio-Harveyi - Sequence and Function of Genes Regulating Expression of Luminescence. *Molecular Microbiology, 9*(4), 773-786. doi:DOI 10.1111/j.1365-2958.1993.tb01737.x

Borlee, B. R., Geske, G. D., Blackwell, H. E., & Handelsman, J. (2010). Identification of Synthetic Inducers and Inhibitors of the Quorum-Sensing Regulator LasR in Pseudomonas aeruginosa by High-Throughput Screening. *Applied and Environmental Microbiology, 76*(24), 8255-8258. doi:10.1128/aem.00499-10

Bottomley, M. J., Muraglia, E., Bazzo, R., & Carfi, A. (2007). Molecular insights into quorum sensing in the human pathogen Pseudomonas aeruginosa from the structure of the virulence regulator LasR bound to its autoinducer. *Journal of Biological Chemistry, 282*(18), 13592-13600. doi:10.1074/jbc.M700556200

Brint, J. M., & Ohman, D. E. (1995). Sythnesis of multiple exoproducts in Pseudomonas-aeruginosa is under the control of the RhlR-RHII, another set of regulators in strain PAO1 with homology to the autoinducer-responsive LuxR-LuxI Family *Journal of Bacteriology, 177*(24), 7155-7163. doi:10.1128/jb.177.24.7155-7163.1995

Cabeen, M. T. (2014). Stationary Phase-Specific Virulence Factor Overproduction by a lasR Mutant of Pseudomonas aeruginosa. *Plos One, 9*(2), 9. doi:10.1371/journal.pone.0088743

Cao, J. G., & Meighen, E. A. (1989). Purification and structural identification of an autoinducer for the luminescence system of Vibrio harveyi. *J Biol Chem, 264*(36), 21670-21676.

Chen, G., Swem, L. R., Swem, D. L., Stauff, D. L., O'Loughlin, C. T., Jeffrey, P. D., . . . Hughson, F. M. (2011). A strategy for antagonizing quorum sensing. *Mol Cell, 42*(2), 199-209. doi:10.1016/j.molcel.2011.04.003

Chhabra, S. R., Harty, C., Hooi, D. S. W., Daykin, M., Williams, P., Telford, G., . . . Bycroft, B. W. (2003). Synthetic analogues of the bacterial signal (quorum sensing) molecule N-(3-oxododecanoyl)-L-homoserine lactone as immune modulators. *Journal of Medicinal Chemistry, 46*(1), 97-104. doi:10.1021/jm020909n

Churchill, M. E. A., & Chen, L. L. (2011). Structural Basis of Acyl-homoserine Lactone-Dependent Signaling. *Chemical Reviews, 111*(1), 68-85. doi:10.1021/cr1000817

DeLano, W. L. (2009). PyMOL molecular viewer: Updates and refinements. *Abstracts of Papers of the American Chemical Society, 238*, 1.

Eberhard, A., Burlingame, A. L., Eberhard, C., Kenyon, G. L., Nealson, K. H., & Oppenheimer, N. J. (1981). Structural identification of autoinducer of Photobacterium fischeri luciferase. *Biochemistry, 20*(9), 2444-2449. doi:10.1021/bi00512a013

Emsley, P., & Cowtan, K. (2004). Coot: model-building tools for molecular graphics. *Acta Crystallogr D Biol Crystallogr, 60*(Pt 12 Pt 1), 2126-2132. doi:10.1107/S0907444904019158

Emsley, P., Lohkamp, B., Scott, W. G., & Cowtan, K. (2010). Features and development of Coot. *Acta Crystallogr D Biol Crystallogr, 66*(Pt 4), 486-501. doi:10.1107/S0907444910007493

Engebrecht, J., Nealson, K., & Silverman, M. (1983). Bacterial bioluminescence: isolation and genetic analysis of functions from Vibrio fischeri. *Cell, 32*(3), 773-781. doi:10.1016/0092-8674(83)90063-6

Feltner, J. B., Wolter, D. J., Pope, C. E., Groleau, M. C., Smalley, N. E., Greenberg, E. P., . . . Dandekar, A. A. (2016). LasR Variant Cystic Fibrosis Isolates Reveal an Adaptable Quorum-Sensing Hierarchy in Pseudomonas aeruginosa. *Mbio, 7*(5), 9. doi:10.1128/mBio.01513-16

Freeman, J. A., Lilley, B. N., & Bassler, B. L. (2000). A genetic analysis of the functions of LuxN: a two-component hybrid sensor kinase that regulates quorum sensing in Vibrio harveyi. *Molecular Microbiology, 35*(1), 139-149. doi:10.1046/j.1365-2958.2000.01684.x

Gambello, M. J., & Iglewski, B. H. (1991). Cloning and characterization of the Pseudomonas aeruginosa lasR gene, a transcriptional activator of elastase expression. *J Bacteriol, 173*(9), 3000-3009.

Gao, J., Ma, A. Z., Zhuang, X. L., & Zhuang, G. Q. (2014). An N-Acyl Homoserine Lactone Synthase in the Ammonia-Oxidizing Bacterium Nitrosospira multiformis. *Applied and Environmental Microbiology, 80*(3), 951-958. doi:10.1128/aem.03361-13

Gerdt, J. P., McInnis, C. E., Schell, T. L., & Blackwell, H. E. (2015). Unraveling the contributions of hydrogen-bonding interactions to the activity of native and non-native ligands in the quorum-sensing receptor LasR. *Organic & Biomolecular Chemistry, 13*(5), 1453-1462. doi:10.1039/c4ob02252a

Gerdt, J. P., McInnis, C. E., Schell, T. L., Rossi, F. M., & Blackwell, H. E. (2014). Mutational Analysis of the Quorum-Sensing Receptor LasR Reveals Interactions that Govern Activation and Inhibition by Nonlactone Ligands. *Chemistry & Biology, 21*(10), 1361-1369.

Gerdt, J. P., Wittenwyler, D. M., Combs, J. B., Boursier, M. E., Brummond, J. W., Xu, H., & Blackwell, H. E. (2017). Chemical Interrogation of LuxR-type Quorum Sensing Receptors Reveals New Insights into Receptor Selectivity and the Potential for Interspecies Bacterial Signaling. *Acs Chemical Biology, 12*(9), 2457-2464. doi:10.1021/acschembio.7b00458

Hanzelka, B. L., Parsek, M. R., Val, D. L., Dunlap, P. V., Cronan, J. E., & Greenberg, E. P. (1999). Acylhomoserine lactone synthase activity of the Vibrio fischeri AinS protein. *Journal of Bacteriology, 181*(18), 5766-5770.

Hawver, L. A., Jung, S. A., & Ng, W. L. (2016). Specificity and complexity in bacterial quorum-sensing systems. *FEMS Microbiol Rev, 40*(5), 738-752. doi:10.1093/femsre/fuw014

Ke, X. B., Miller, L. C., & Bassler, B. L. (2015). Determinants governing ligand specificity of the Vibrio harveyi LuxN quorum-sensing receptor. *Molecular Microbiology, 95*(1), 127-142. doi:10.1111/mmi.12852

Kukavica-Ibrulj, I., Bragonzi, A., Paroni, M., Winstanley, C., Sanschagrin, F., O'Toole, G. A., & Levesque, R. C. (2008). In vivo growth of Pseudomonas aeruginosa strains PAO1 and PA14 and the hypervirulent strain LESB58 in a rat model of chronic lung infection. *Journal of Bacteriology, 190*(8), 2804-2813. doi:10.1128/jb.01572-07

Latifi, A., Winson, M. K., Foglino, M., Bycroft, B. W., Stewart, G. S. A. B., Lazdunski, A., & Williams, P. (1995). Multiple Homologs of Luxr and Luxl Control Expression of Virulence Determinants and Secondary Metabolites through Quorum Sensing in Pseudomonas-Aeruginosa Pao1. *Molecular Microbiology, 17*(2), 333-343. doi:DOI 10.1111/j.1365-2958.1995.mmi_17020333.x

Mellbye, B. L., Spieck, E., Bottomley, P. J., & Sayavedra-Soto, L. A. (2017). Acyl-Homoserine Lactone Production in Nitrifying Bacteria of the Genera Nitrosospira, Nitrobacter, and Nitrospira Identified via a Survey of Putative Quorum-Sensing Genes. *Applied and Environmental Microbiology, 83*(22), 13. doi:10.1128/aem.01540-17

Michael, B., Smith, J. N., Swift, S., Heffron, F., & Ahmer, B. M. (2001). SdiA of Salmonella enterica is a LuxR homolog that detects mixed microbial communities. *J Bacteriol, 183*(19), 5733-5742. doi:10.1128/JB.183.19.5733-5742.2001

Minor, W., Cymborowski, M., Otwinowski, Z., & Chruszcz, M. (2006). HKL-3000: the integration of data reduction and structure solution--from diffraction images to an initial model in minutes. *Acta Crystallogr D Biol Crystallogr, 62*(Pt 8), 859-866. doi:10.1107/S0907444906019949

Mukherjee, S., Moustafa, D., Smith, C. D., Goldberg, J. B., & Bassler, B. L. (2017). The RhlR quorum-sensing receptor controls Pseudomonas aeruginosa pathogenesis and biofilm development independently of its canonical homoserine lactone autoinducer. *Plos Pathogens, 13*(7), 25. doi:10.1371/journal.ppat.1006504

Nasser, W., & Reverchon, S. (2007). New insights into the regulatory mechanisms of the LuxR family of quorum sensing regulators. *Analytical and Bioanalytical Chemistry, 387*(2), 381-390. doi:10.1007/s00216-006-0702-0

Nguyen, Y., Nguyen, N. X., Rogers, J. L., Liao, J., MacMillan, J. B., Jiang, Y., & Sperandio, V. (2015). Structural and mechanistic roles of novel chemical ligands on the SdiA quorum-sensing transcription regulator. *MBio, 6*(2). doi:10.1128/mBio.02429-14

O'Loughlin, C. T., Miller, L. C., Siryaporn, A., Drescher, K., Semmelhack, M. F., & Bassler, B. L. (2013). A quorum-sensing inhibitor blocks Pseudomonas aeruginosa virulence and biofilm formation. *Proceedings of the National Academy of Sciences of the United States of America, 110*(44), 17981-17986. doi:10.1073/pnas.1316981110

Paczkowski, J. E., Mukherjee, S., McCready, A. R., Cong, J. P., Aquino, C. J., Kim, H., . . . Bassler, B. L. (2017). Flavonoids Suppress Pseudomonas aeruginosa Virulence through Allosteric Inhibition of Quorum-sensing Receptors. *J Biol Chem, 292*(10), 4064-4076. doi:10.1074/jbc.M116.770552

Papenfort, K., & Bassler, B. L. (2016). Quorum sensing signal-response systems in Gram-negative bacteria. *Nature Reviews Microbiology, 14*(9), 576-588. doi:10.1038/nrmicro.2016.89

Pearson, J. P., Gray, K. M., Passador, L., Tucker, K. D., Eberhard, A., Iglewski, B. H., & Greenberg, E. P. (1994). Structure of the autoinducer required for expression of Pseudomonas aeruginosa virulence genes. *Proc Natl Acad Sci U S A, 91*(1), 197-201. doi:10.1073/pnas.91.1.197

Pearson, J. P., Pesci, E. C., & Iglewski, B. H. (1997). Roles of Pseudomonas aeruginosa las and rhl quorum-sensing systems in control of elastase and rhamnolipid biosynthesis genes. *Journal of Bacteriology, 179*(18), 5756-5767.

Rampioni, G., Schuster, M., Greenberg, E. P., Bertani, I., Grasso, M., Venturi, V., . . . Leoni, L. (2007). RsaL provides quorum sensing homeostasis and functions as a global regulator of gene expression in Pseudomonas aeruginosa. *Molecular Microbiology, 66*(6), 1557-1565. doi:10.1111/j.1365-2958.2007.06029.x

Schuster, M., & Greenberg, E. P. (2007). Early activation of quorum sensing in Pseudomonas aeruginosa reveals the architecture of a complex regulon. *Bmc Genomics, 8*, 11. doi:10.1186/1471-2164-8-287

Schuster, M., Urbanowski, M. L., & Greenberg, E. P. (2004). Promoter specificity in Pseudomonas aeruginosa quorum sensing revealed by DNA binding of purified LasR. *Proceedings of the National Academy of Sciences of the United States of America, 101*(45), 15833-15839. doi:10.1073/pnas.0407229101

Schweizer, H. P. (1991). Escherichia-Pseudomonas shuttle vectors derived from pUC18/19. *Gene, 97*(1), 109-121. doi:10.1016/0378-1119(91)90016-5

Simon, R., Priefer, U., & Puhler, A. (1983). A Broad Host Range Mobilization System for Invivo Genetic-Engineering - Transposon Mutagenesis in Gram-Negative Bacteria. *Bio-Technology, 1*(9), 784-791. doi:DOI 10.1038/nbt1183-784

Sitnikov, D. M., Schineller, J. B., & Baldwin, T. O. (1996). Control of cell division in Escherichia coli: regulation of transcription of ftsQA involves both rpoS and SdiA-mediated autoinduction. *Proc Natl Acad Sci U S A, 93*(1), 336-341.

Smalley, N. E., An, D. D., Parsek, M. R., Chandler, J. R., & Dandekar, A. A. (2015). Quorum Sensing Protects Pseudomonas aeruginosa against Cheating by Other Species in a Laboratory Coculture Model. *Journal of Bacteriology, 197*(19), 3154-3159. doi:10.1128/jb.00482-15

Tashiro, Y., Yawata, Y., Toyofuku, M., Uchiyama, H., & Nomura, N. (2013). Interspecies Interaction between Pseudomonas aeruginosa and Other Microorganisms. *Microbes and Environments, 28*(1), 13-24. doi:10.1264/jsme2.ME12167

Vannini, A., Volpari, C., Gargioli, C., Muraglia, E., Cortese, R., De Francesco, R., . . . Di Marco, S. (2002). The crystal structure of the quorum sensing protein TraR bound to its autoinducer and target DNA. *Embo Journal, 21*(17), 4393-4401. doi:10.1093/emboj/cdf459

You, Y. S., Marella, H., Zentella, R., Zhou, Y. Y., Ulmasov, T., Ho, T. H. D., & Quatrano, R. S. (2006). Use of bacterial quorum-sensing components to regulate gene expression in plants. *Plant Physiology, 140*(4), 1205-1212. doi:10.1104/pp.105.074666

Zhang, R. G., Pappas, K. M., Pappas, T., Brace, J. L., Miller, P. C., Oulmassov, T., . . . Joachimiak, A. (2002). Structure of a bacterial quorum-sensing transcription factor complexed with pheromone and DNA. *Nature, 417*(6892), 971-974. doi:10.1038/nature00833

Zhu, J., & Winans, S. C. (2001). The quorum-sensing transcriptional regulator TraR requires its cognate signaling ligand for protein folding, protease resistance, and dimerization. *Proc Natl Acad Sci U S A, 98*(4), 1507-1512. doi:10.1073/pnas.98.4.1507

Figures and Figure Legends

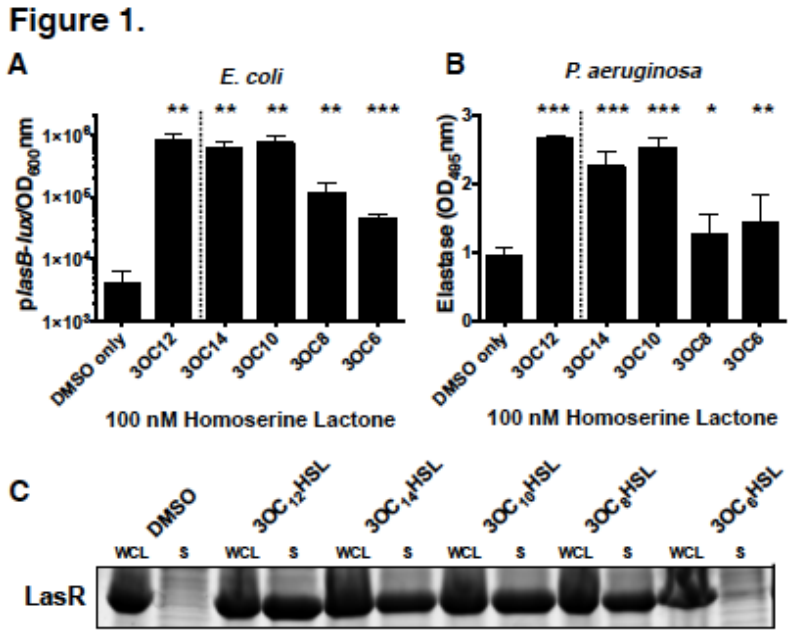

Figure 1. *LasR is activated by multiple homoserine lactone autoinducers.* A) LasR-dependent bioluminescence was measured in *E. coli*. Arabinose-inducible LasR was produced from one plasmid and the p*lasB-lux* reporter construct was carried on a second plasmid. 0.1% arabinose was used for LasR induction. B) Elastase activity was measured from Δ*lasI P. aeruginosa* using elastin-Congo red as the substrate. In A and B, 100 nM of the designated HSLs were tested. Two technical replicates were performed for each biological sample and 3 biological replicates were assessed. Error bars denote standard deviations of the mean. Paired 2-tailed t-tests were performed comparing each compound to the DMSO control. P-values: * <.05, ** <.01, *** <.0001. In panels A and B, we have separated the DMSO control and the results with the cognate autoinducer $3OC_{12}HSL$ by the dotted vertical line. C) Comparison of LasR LBD protein levels in whole cell lysates (WCL) and in the soluble fractions (S) of *E. coli* cells that harbor the DNA encoding the

LasR LBD on a plasmid. 1 mM IPTG was used for LasR LBD induction and either 1% DMSO or 10 μM of the indicated HSL was supplied. In all lanes, protein from .05 OD of cells was loaded. Results are representative of 3 trials.

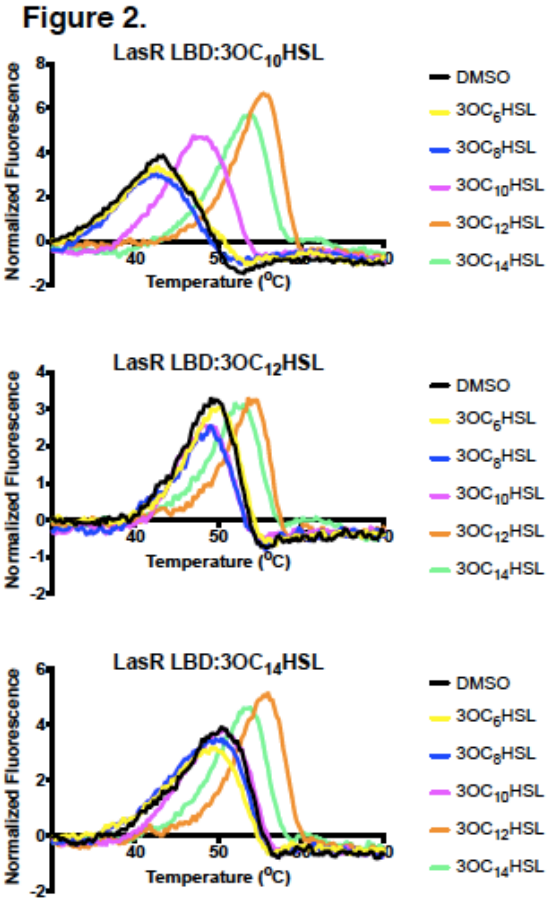

Figure 2. *LasR is stable when bound to long chain HSLs.* Thermal shift analyses of purified LasR LBD bound to $3OC_{10}HSL$ (top), $3OC_{12}HSL$ (middle), and $3OC_{14}HSL$ (bottom) without (designated DMSO) and following supplementation with an additional 10 μM of the indicated HSLs. Each line represents the average of 3 replicates.

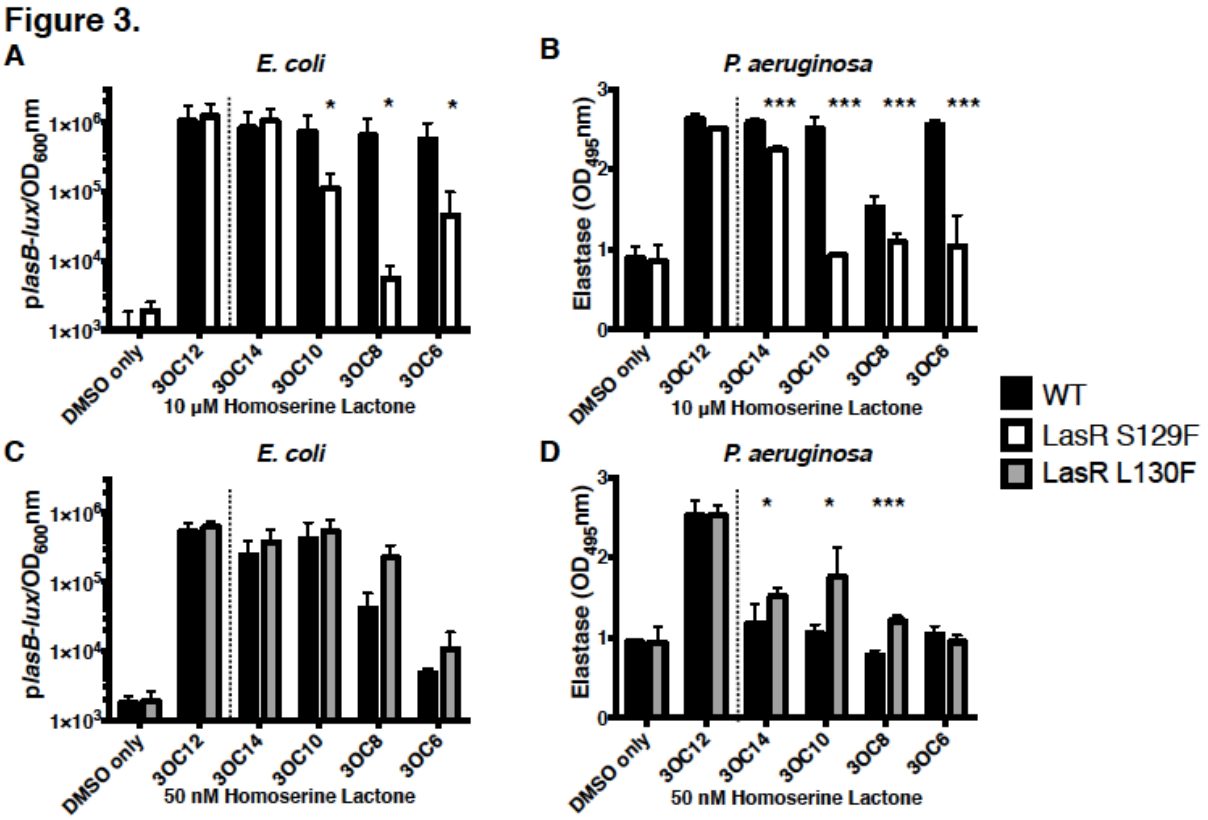

Figure 3. *LasR S129F and LasR L130F alter LasR sensitivity to HSL autoinducers*. A) Wildtype LasR and LasR S129F-driven bioluminescence from the *E. coli* p*lasB-lux* reporter (see Figure 1, panel A for detail). B) Wildtype LasR and LasR S129F-driven elastase activity in Δ*lasI P. aeruginosa* (see Figure 1, panel B for detail). In A and B, 10 μM of the indicated HSLs were provided. C and D) As in panels A and B, respectively, with wildtype LasR and LasR L130F and 50 nM of the indicated HSLs. Black bars, wildtype LasR; white bars, LasR S129F; gray bars, LasR L130F. Two technical replicates were performed for each biological sample and 3 biological replicates were assessed. Error bars denote standard deviations of the mean. Unpaired 2-tailed T-tests were performed comparing WT LasR to the mutant LasR for each compound. p-values: * < .05,

*** <.001. In all panels, we have separated the DMSO control and the results with the cognate autoinducer $3OC_{12}HSL$ by the dotted vertical line.

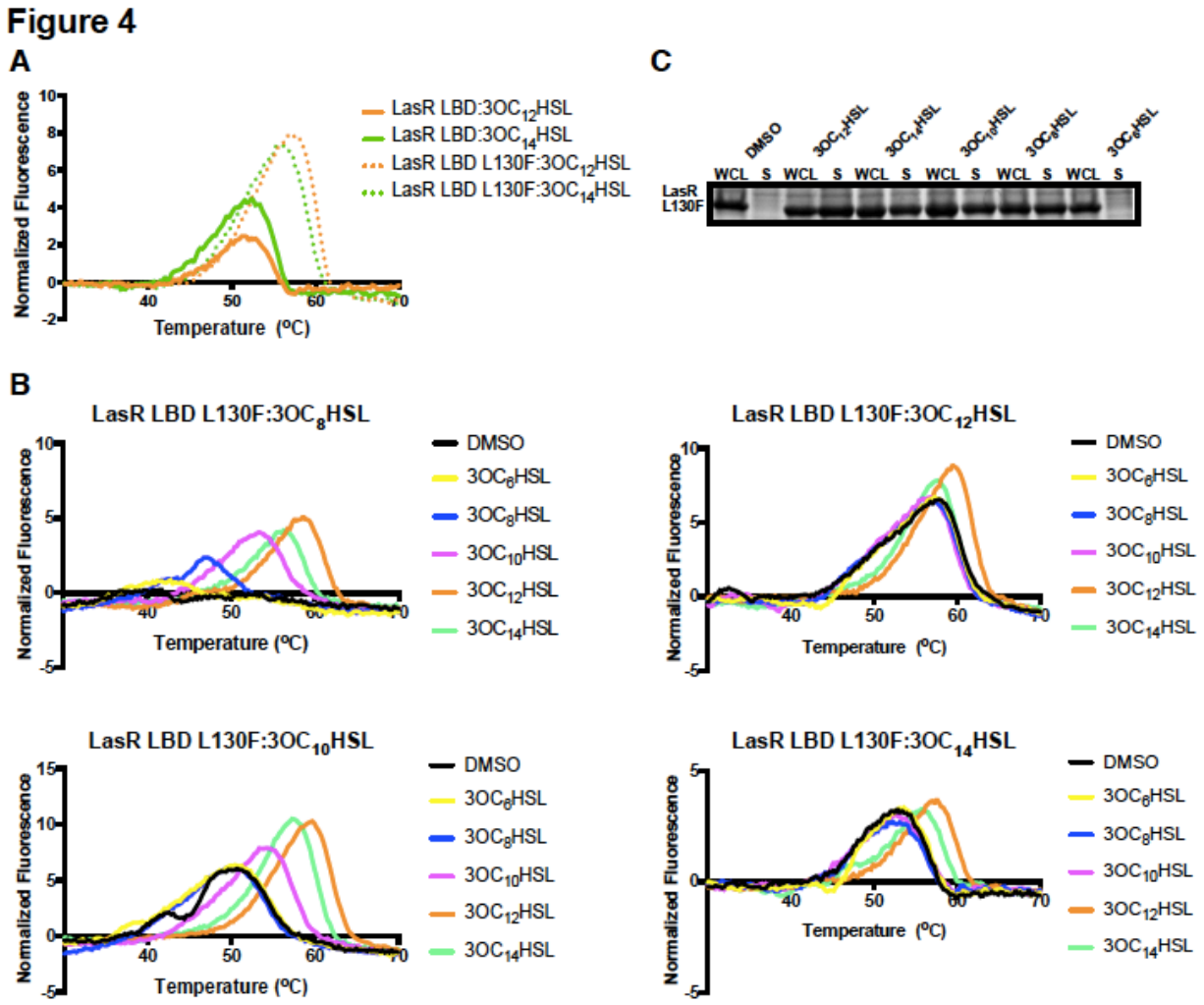

Figure 4. *The LasR LBD L130F is more stable than the wildtype LasR LBD.* A) Thermal shift analyses of purified LasR LBD (solid lines) and LasR LBD L130F (dotted lines) bound to $3OC_{12}HSL$ (orange) or $3OC_{14}HSL$ (green). Each line represents the average of 3 replicates. B) Thermal shift analyses of purified LasR LBD L130F bound to $3OC_{8}HSL$ (top left), $3OC_{10}HSL$ (bottom left), $3OC_{12}HSL$ (top right), and $3OC_{14}HSL$ (bottom right) without (designated DMSO) and following supplementation with an additional 10 μM of the indicated HSLs. C) Comparison of LasR L130F levels in the whole cell lysates (WCL) and the soluble fractions (S) of *E. coli* cells harboring the DNA encoding LasR LBD L130F on

a plasmid (see Figure 1, panel C for details). Either 1% DMSO or 10 μM of the indicated HSL molecule was added.

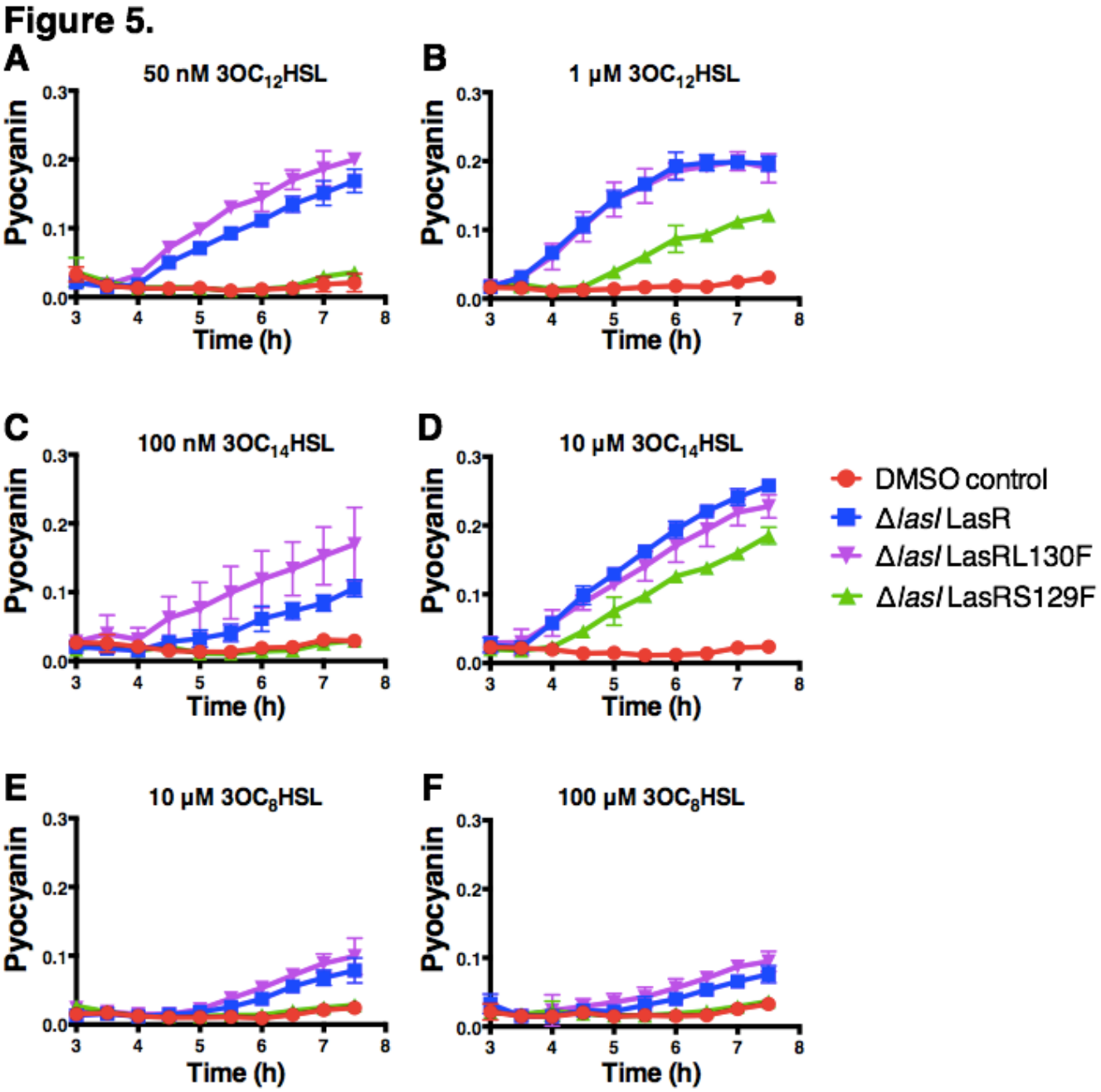

Figure 5. *Wildtype LasR, LasR S129F, and LasR L130F display distinct pyocyanin production phenotypes in response to different HSL autoinducers.* Pyocyanin production was measured spectophotometrically in Δ*lasI P. aeruginosa* over the growth curve. Y-axis "Pyocyanin" is the amount of pyocyanin pigment (OD_{695} nm) over cell density (OD_{600} nm). Designations are: red, DMSO control; blue, wildtype LasR; purple, LasR L130F;

green, LasR S129F. Data show the mean of 3 biological replicates. Error bars denote standard deviations of the mean. Concentrations and ligands used are: A) 50 nM $3OC_{12}HSL$, B) 1 μM $3OC_{12}HSL$, C) 100 nM $3OC_{14}HSL$, D) 10 μM $3OC_{14}HSL$, E) 10 μM $3OC_8HSL$, and F) 100 μM $3OC_8HSL$

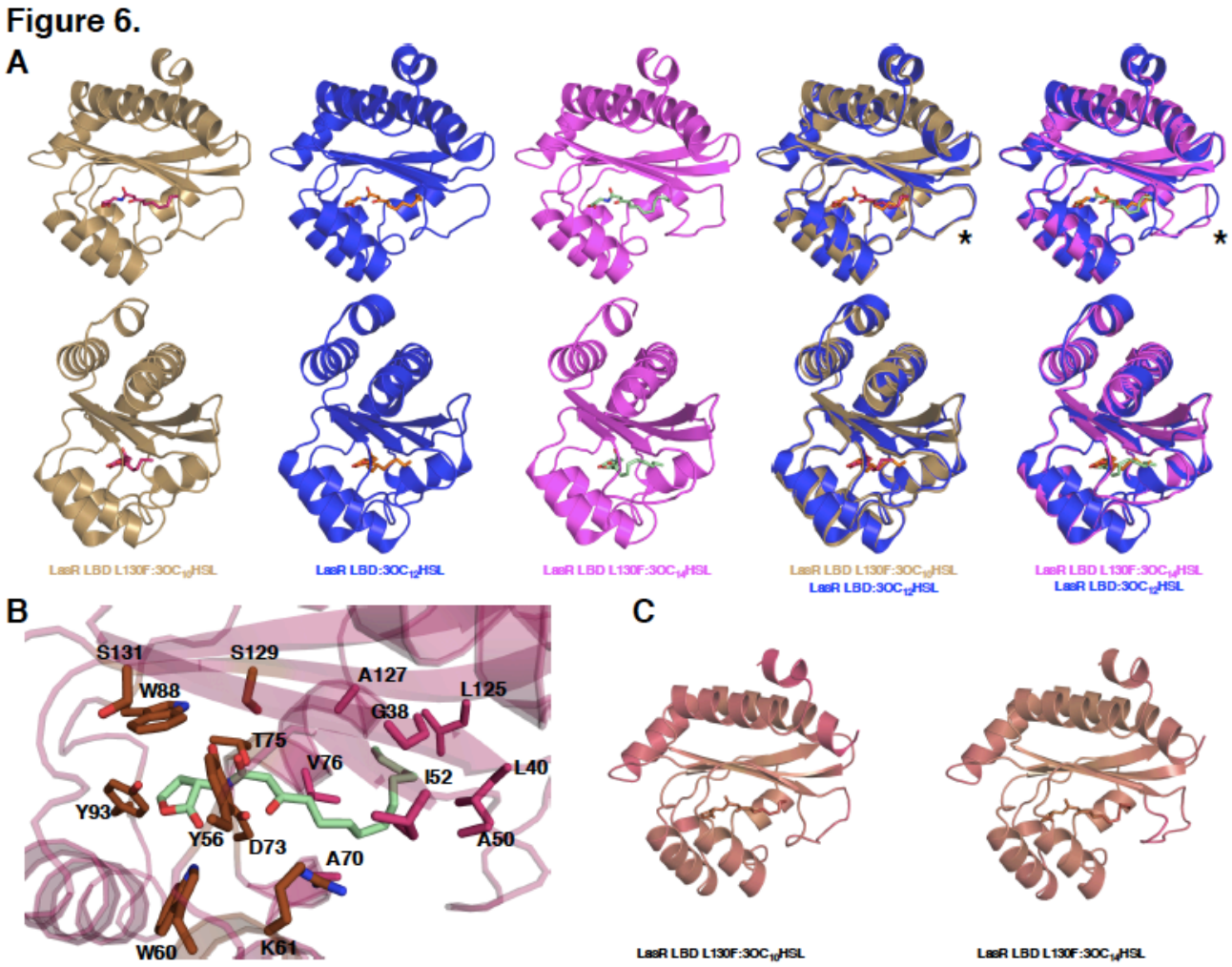

Figure 6. *Crystal structures of LasR LBD L130F bound to 3OC$_{10}$HSL and 3OC$_{14}$HSL*. A) Crystal structures of LasR LBD L130F:3OC$_{10}$HSL (gold) and LasR LBD L130F:3OC$_{14}$HSL (magenta) compared to the wildtype LasR LBD:3OC$_{12}$HSL structure (blue, modified from Bottomley et al. 2007, PBD: 2UVO). The bottom images show 90-degree rotations of the crystal structures relative to the images above. In the top right-most 2 structures, the asterisks highlight the LasR loop region that includes residues 40-52 and that undergoes a conformational shift when 3OC$_{14}$HSL is bound. B) LasR LBD L130F:3OC$_{14}$HSL crystal structure (protein: magenta, ligand: green). Amino acids drawn in stick format show

important residues for lactone head binding (Y56, W60, K61, D73, T75, W88, Y93, S129, and S131, all colored in brown) and acyl tail binding (G38, L40, A50, I52, A70, V76, L125, and A127, all colored in pink). C) Comparison of the average B-factors for LasR LBD L130F bound to $3OC_{10}HSL$ and bound to $3OC_{14}HSL$. The structures are colored from gold to magenta with gold representing the lowest average B-factor and magenta representing the highest average B-factor.

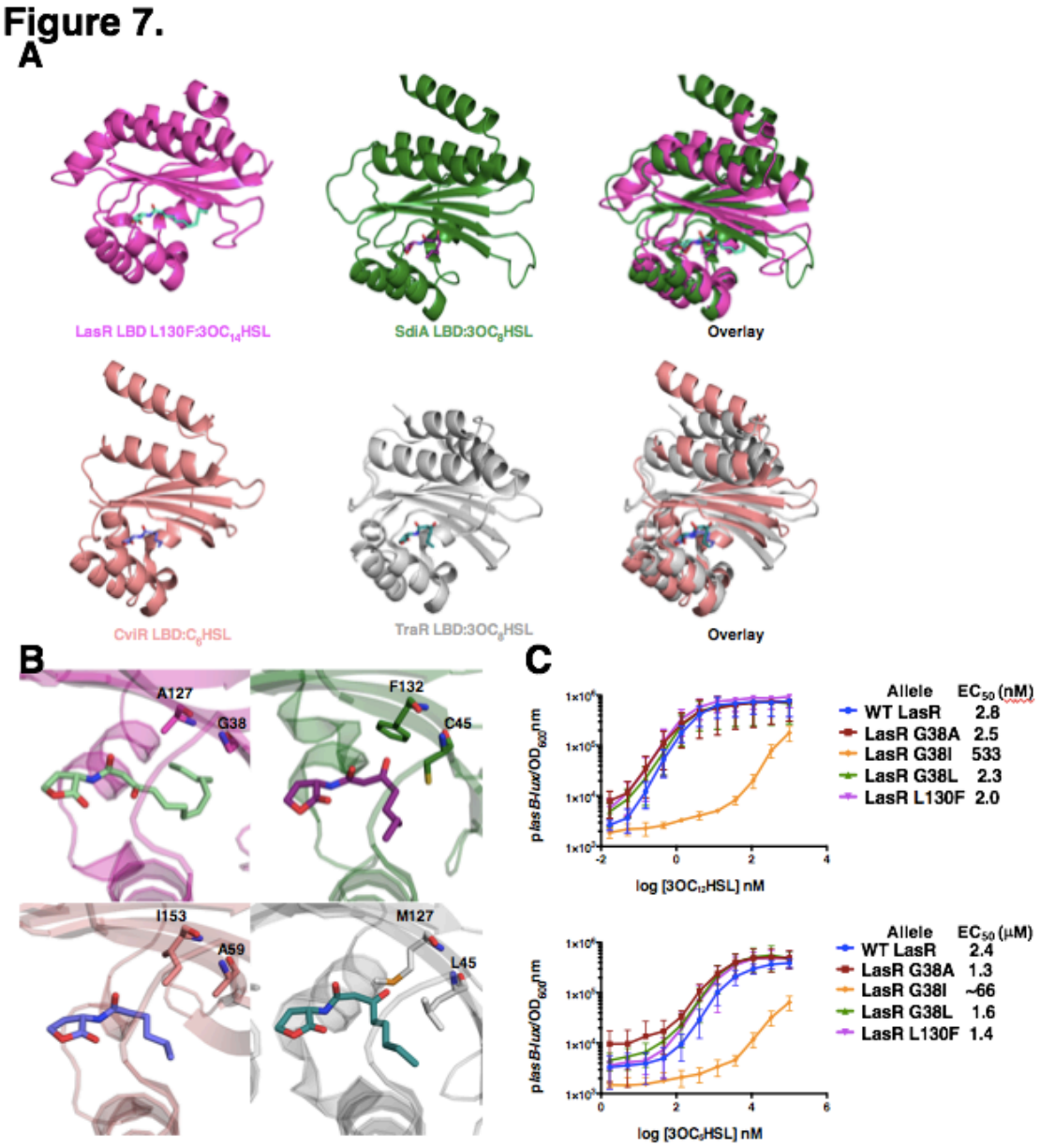

Figure 7. *A conserved flexible loop region confers promiscuity to LuxR-type receptors.* A) Top images: structural comparison of the LuxR-type receptors LasR LBD L130F:3OC$_{14}$HSL (magenta) and SdiA LBD:3OC$_{8}$HSL (green, modified from Nguyen et al., 2015, PDB: AY17) that exhibit promiscuity with respect to ligand binding. Bottom images: structural comparison of the LuxR-type receptors CviR LBD:C$_{6}$HSL (pink,

modified from Chen et al., 2011, PDB: 3QP1) and TraR LBD:3OC$_8$HSL (silver, modified from Zhang et al., 2002, PDB: 1L3L) that display strict ligand specificity. B) Structural comparison of the protein:ligand interfaces for LasR LBD L130F:3OC$_{14}$HSL (top left, magenta), SdiA LBD:3OC$_8$HSL (top right, green), CviR LBD:C$_6$HSL (bottom left, pink), and TraR LBD:3OC$_8$HSL (bottom right, silver). Residues that make important hydrophobic sidechain interactions in each protein:ligand complex are shown in stick format and named. C) Dose response curves from the *E. coli* p*lasB-lux* reporter assay (see Figure 1, panel A) were used to determine EC$_{50}$ values for 3OC$_{12}$HSL (top panel) and 3OC$_6$HSL (bottom panel) for wildtype LasR (blue), LasR G38A (dark red), LasR G38I (orange), LasR G38L (dark green), and LasR L130F (magenta). Two technical replicates were performed for each biological sample and 3 biological replicates were assessed. Error bars denote standard deviations of the mean.

Table 1. EC_{50} (nM) values for LasR and HSL compounds in the *plasB-lux* assay

LasR Allele

	WT	S129C	S129W	S129F	S129T	S129M	L130F
$3OC_{12}HSL$	2.8	5.9	76.8	177	870	6570	2.0
$3OC_{14}HSL$	6.2	11.8	12.8	41.2	4070	NR	5.3
$3OC_{10}HSL$	8.0	31.5	2620	4980	4510	NR	5.0
$3OC_{8}HSL$	885	2860	2180	NR	NR	NR	80.7
$3OC_{6}HSL$	2370	4400	NR	55600	71700	NR	1390

NR denotes non-responsive

Supplementary Figures and Figure Legends

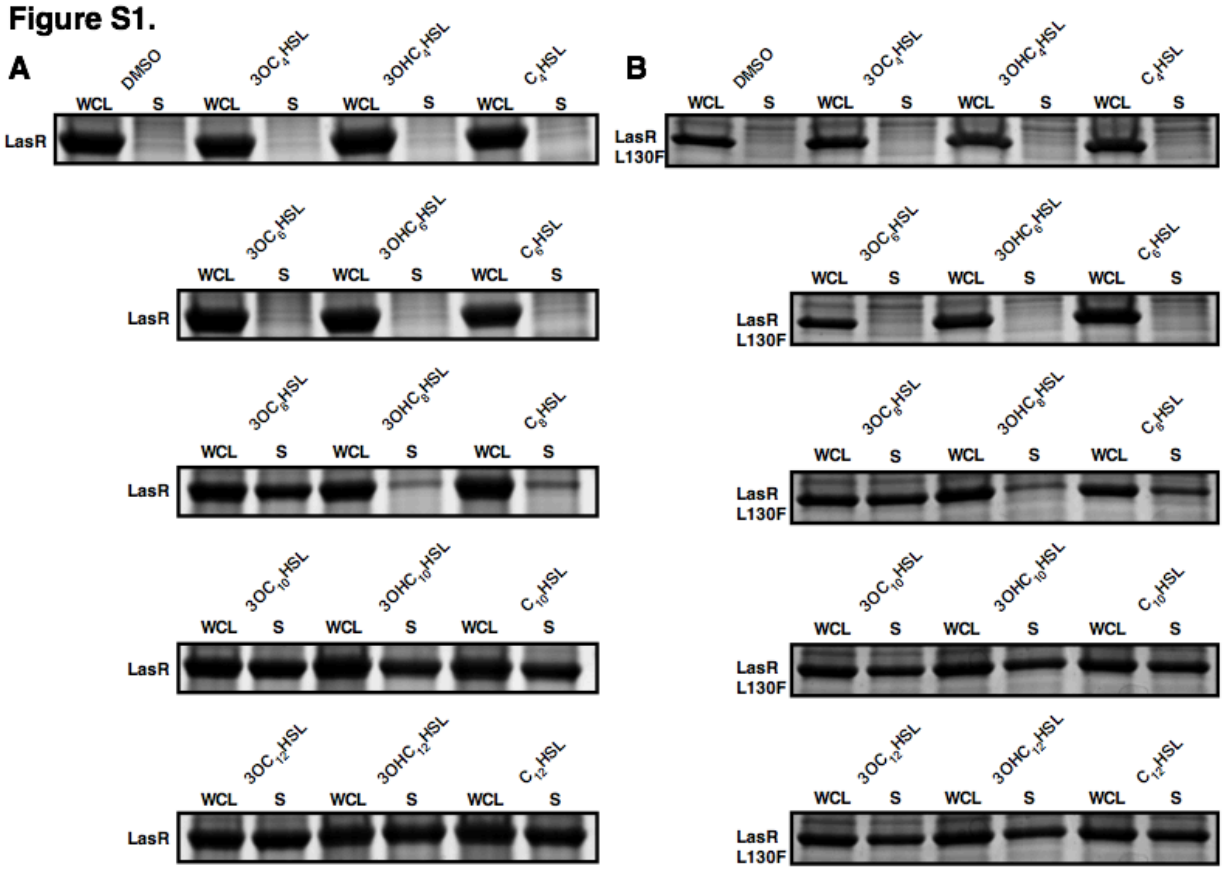

Figure S1. *Long acyl chain HSLs solubilize the LasR LBD and the LasR LBD L130F.* Comparison of wildtype LasR LBD protein levels in whole cell lysates (WCL) and in the soluble fractions (S) of *E. coli* cells harboring the DNA encoding the LasR LBD on a plasmid. B) As in panel A with LasR LBD L130F. In both panels, 1 mM IPTG was used for LasR induction and either 1% DMSO or 10 μM of the indicated HSL was added. See Figure 1, panel C of the main text for details.

Table S1. EC_{50} (nM) values for LasR and HSL compounds in the *plasB-lux* assay

Ligand	LasR Allele							
	WT	S129C	S129W	S129F	S129T	S129M	L128F	L130F
$3OC_{12}HSL$	2.8	5.9	76.8	177	870	6570	3.12	2.0
$3OHC_{12}HSL$	39.3	174	319	2920	NR	NR	37.3	23.4
$C_{12}HSL$	10.1	71.0	629	941	970	NR	5.1	6.3
$3OC_{14}HSL$	6.2	11.8	12.8	41.2	4070	NR	2.9	5.3
$C_{14}HSL$	25.9	57.5	64.2	NR	NR	NR	9.5	13.2
$3OC_{10}HSL$	8.0	31.5	2620	4980	4510	NR	5.3	5.0
$3OHC_{10}HSL$	271	1470	38700	NR	NR	NR	563	112
$C_{10}HSL$	401	4220	NR	NR	NR	NR	1192	172
$3OC_{8}HSL$	885	2860	2180	NR	NR	NR	1127	80.7
$3OHC_{8}HSL$	37300	NR	NR	NR	NR	NR	67000	17100
$C_{8}HSL$	27000	NR	NR	NR	NR	NR	4000	5930
$3OC_{6}HSL$	2370	4400	NR	55600	71700	NR	1230	1390
$3OHC_{6}HSL$	19900	NR	NR	NR	NR	NR	20100	2220

NR denotes non-responsive

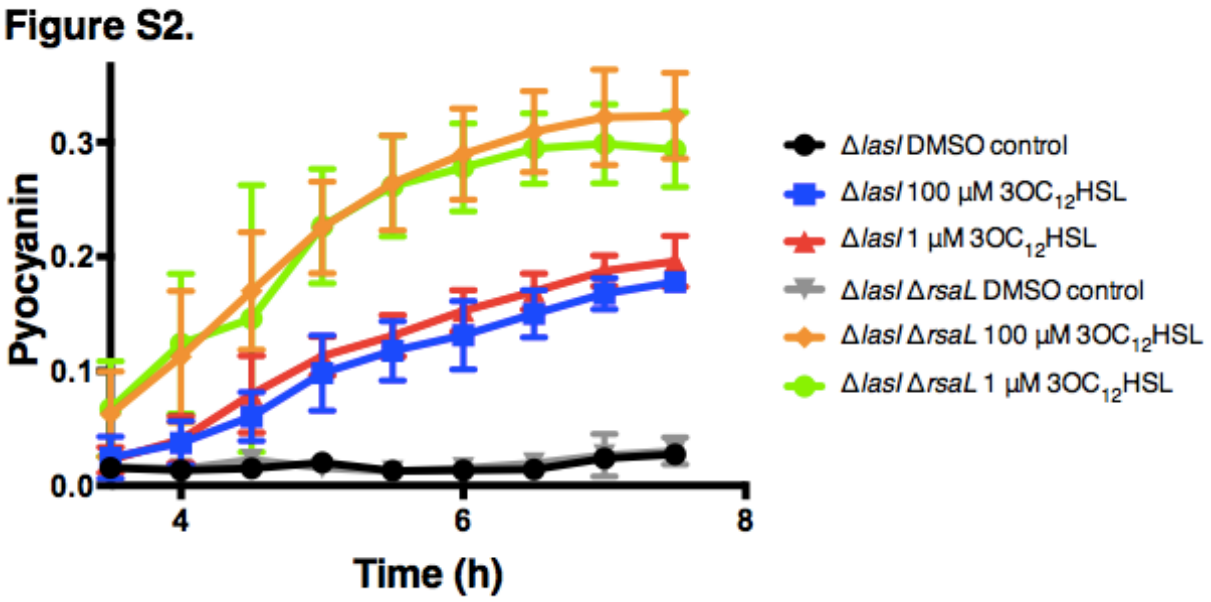

Figure S2. *RsaL is required for inhibition of pyocyanin production by high HSL concentrations in P. aeruginosa.* Pyocyanin production was measured spectophotometrically from *P. aeruginosa* Δ*lasI* and Δ*lasI* Δ*rsaL* strains over the growth curve following addition of DMSO, 1 μM $3OC_{12}HSL$, or 100 μM $3OC_{12}HSL$ as indicated. Y-axis "Pyocyanin" is the amount of pyocyanin pigment (OD_{695} nm) over cell density (OD_{600} nm). Data show the mean of 3 biological replicates. Error bars denote standard deviations of the mean.

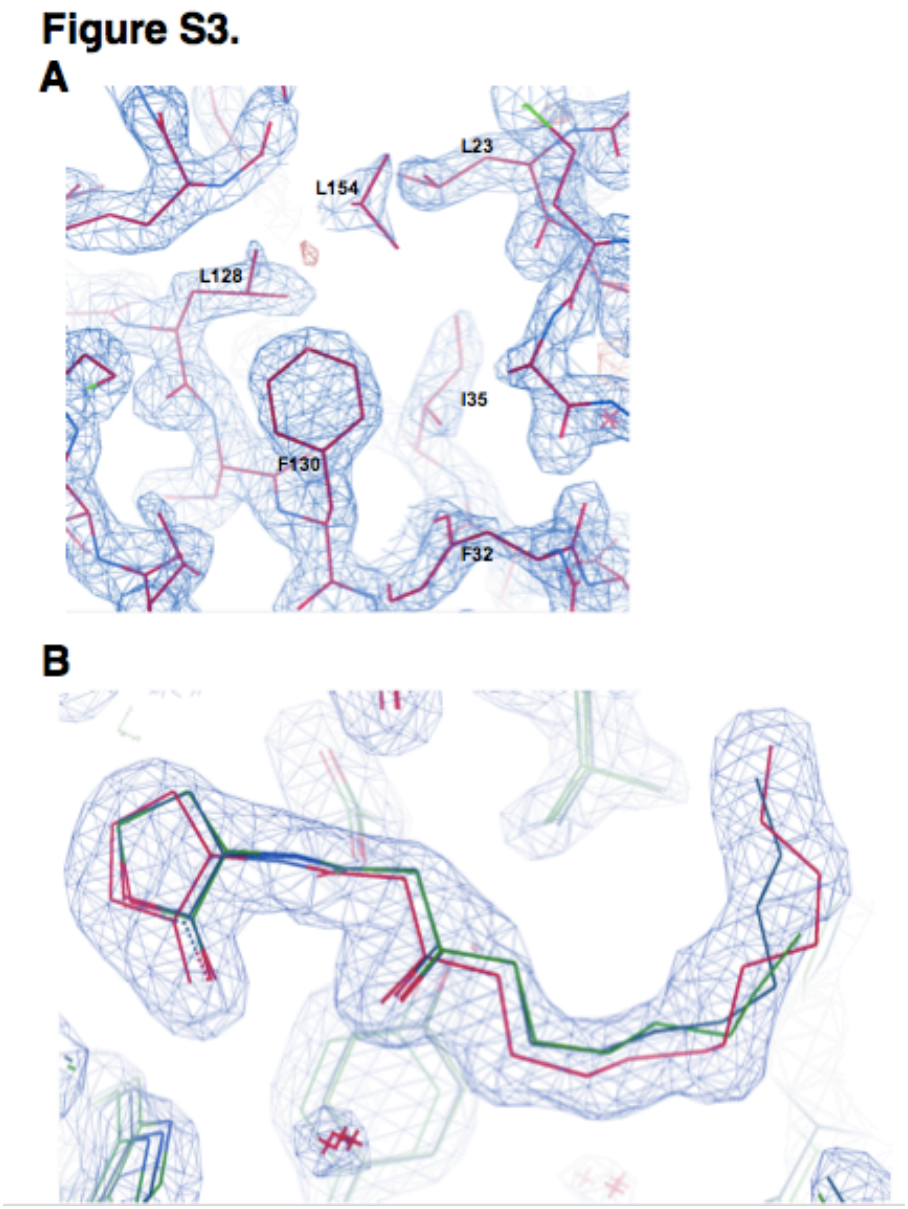

Figure S3. *Electron density for LasR LBD L130F near residue F130 and the 3OC$_{14}$HSL ligand.* A) A simulated annealing omit map, contoured at 1σ, shows the electron density around LasR residue F130 and the surrounding hydrophobic residues. F130 interacts with L23, L30, F32, I35, L114, L118, L128, L151, and L154 in the LasR LBD L130F:3OC$_{14}$HSL structure. The panel depicts the perspective highlighting the F130 interactions with L23, F32, I35, L128, and L154, and these residues are labeled. B) A

simulated annealing omit map, contoured at 1σ, shows the electron density around the HSLs in the LasR LBD bound to $3OC_{10}HSL$ (green), $3OC_{14}HSL$ (red), or $3OC_{12}HSL$ (blue, from data in Bottomley *et al*., 2007).

Figure S4.

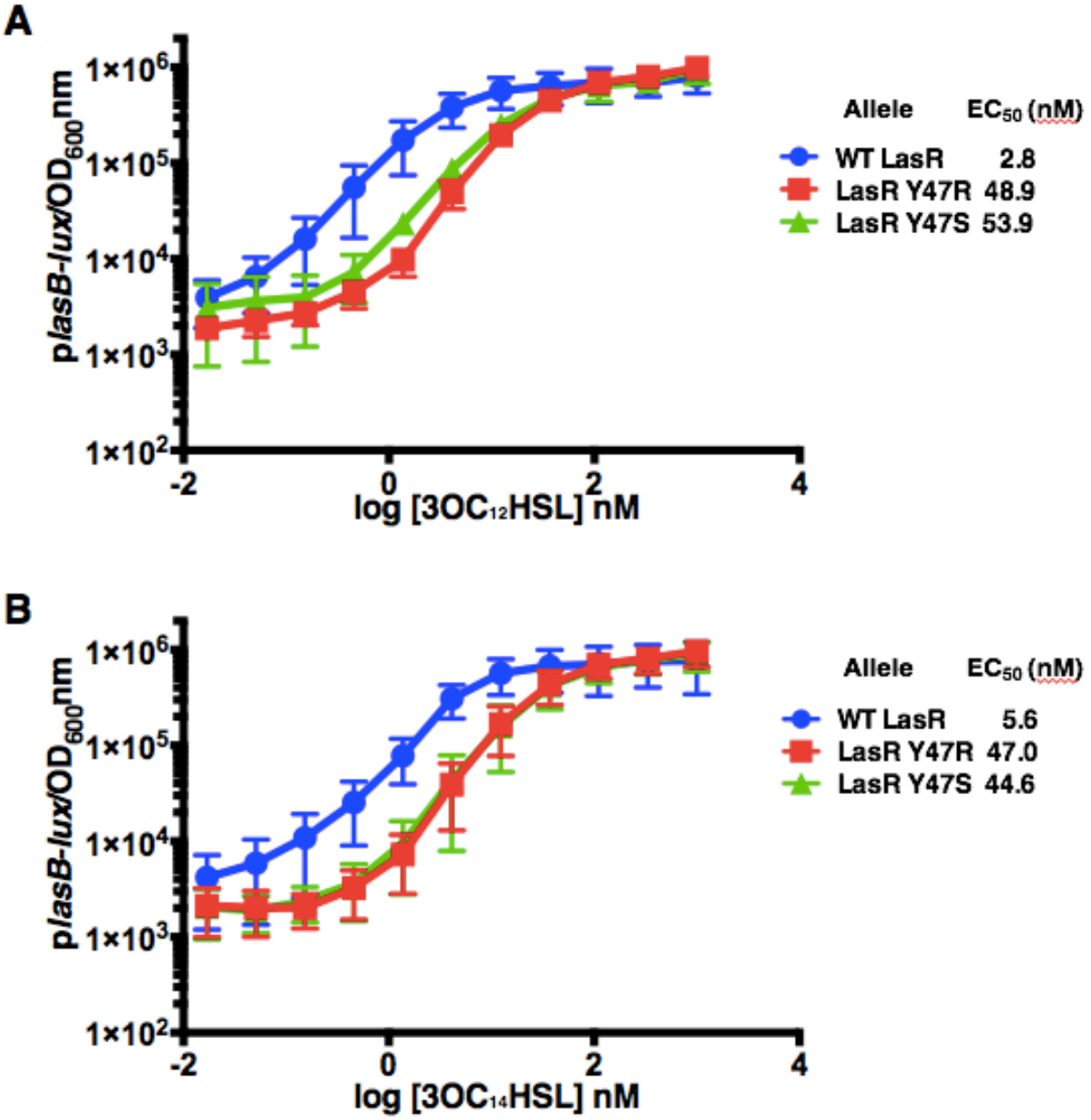

Figure S4. *LasR Y47R and LasR Y47S have lower affinities for 3OC$_{12}$HSL and 3OC$_{14}$HSL than wildtype LasR.* Bioluminescence from the p*lasB-lux* reporter driven by wildtype LasR (blue), LasR Y47R (red), and LasR Y47S (green) (See Figure 1, panel A of the main text for details). 3OC$_{12}$HSL (A) or 3OC$_{14}$HSL (B) were added at the designated

concentrations. Two technical replicates were performed for each biological sample and 3 biological replicates were assessed. Error bars depict standard deviations of the mean.